Bonding in Ground-State and Excited-State A^+·Rg van der Waals Ions (A = Atom, Rg = Rare-Gas Atom): A Model-Potential Analysis

D. Bellert and W. H. Breckenridge*

Department of Chemistry, University of Utah, 315 South 1400 East, Room 2020, Salt Lake City, Utah 84112

Received September 10, 2001

Contents

I. Introduction

Solvation of positive atomic ions A^+ is extremely important in many areas, ranging from basic inorganic chemistry and electrochemistry to biochemistry. In recent years several fundamental theoretical and experimental studies of the bonding of solvent molecules to such A^+ centers in the gas phase have been conducted, with particular emphasis on the changes in bond strength as one, two, three, etc., molecules solvate the ion. The simplest interaction is that of an A^+ atomic ion with one molecule (= solvent), and it is obvious that a fundamental step in understanding the interactions of an A^+ ion with a "sea" of solvent molecules is to understand in detail the interactions of A^+ with one solvent molecule. This is most easily studied, of course (both theoretically and experimentally), and there is a large body of literature on themes related to $A^+(solvent)_1$ interactions. Experimentally, sophisticated laser, molecular ion-beam, and mass-spectrometric techniques have been developed in the past several years which have resulted in a wealth of information about $A^+(solvent)_1$ bonding interactions.

The simplest of all solvents for A^+ ions are closed-shell atoms, particularly the rare-gas (Rg) atoms He,

* To whom correspondence should be addressed. Phone: 801-581-8024, Fax: 801-587-9919. E-mail: breck@chem.utah.edu.

10.1021/cr980090e CCC: $39.75
Published on Web 04/04/2002

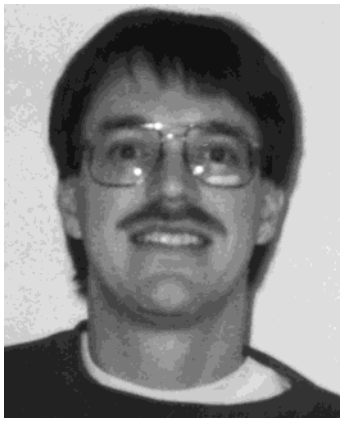

Darrin Bellert was born on April 9, 1968, the second of six children. He attended Carroll High School in Dayton, OH, where the seeds of scientific curiosity were planted. Having graduated in 1986, he enrolled at Wright State University and was befriended by Dr. Paul Seybold, a physical chemist who nurtured this young scientist. After receiving a Bachelor of Science degree, Bellert continued his pursuit of scientific knowledge at the University of Florida. He joined the research group of Dr. Phillip Brucat (a true master of experimental physical chemistry) and performed many spectroscopic studies of transition-metal cations bound to rare-gas atoms and small molecules (some of which are discussed in this review), receiving his Ph.D. degree in 1998. Currently, Bellert is an Assistant Research Professor at the University of Utah and is thrilled to work with yet another great scientist, Bill Breckenridge, as he continues doing elegant spectroscopic studies of gaseous molecules.

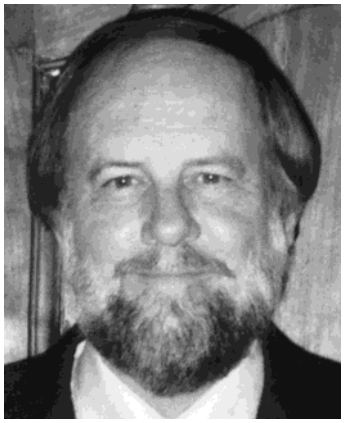

W. H. (Bill) Breckenridge was born on October 14, 1941, graduated from Louisburg Rural High School in 1959, and then immersed himself—as a somewhat naive freshman—in the rigorous, innovative Honors Program at the University of Kansas; enjoying the intellectual challenges (and eventual encouragement) of both english and chemistry professors (particularly Sherry Rowland, whose research group he eventually joined), he found he soon had two sets of friends, a slide-rule-on-the-belt bunch (sometimes a bit boring) and a rag-tag, raucous group of humanities majors. He finally decided (as a Senior) to major in chemistry rather than english, a decision he has never regretted. Breckenridge was fortunate enough to win a Fulbright Fellowship for a year of graduate study in physical chemistry at the University of Leeds in 1963–64, doing gas-phase photochemistry with Fred Dainton and Don Baulch. He then returned to the United States to do his Ph.D. work at Stanford University with Henry Taube (who was sufficiently kind and broad-minded to let this physical chemist develop his own ideas and skills in an inorganic, wonderfully eclectic research group). After an interesting NATO postdoctoral year doing flash photolysis with Tony Callear at Cambridge University in 1969, Breckenridge spent a productive 1–1/2 years as a Member of Technical Staff at Bell Labs in Murray Hill, NJ, with Terry Miller's research group, doing gas-phase flow-tube kinetics using EPR techniques. In 1971, he joined the faculty of the Department of Chemistry at the University of Utah. Thirty years later, he is still there as a Professor of Chemistry, quite happily pursuing his research and teaching efforts as he nears retirement. With essentially "pure" research support (from NSF and PRF), he has conducted many fundamental studies in dynamics and spectroscopy in the gas phase (resulting in over 140 publications), has had the real pleasure of interacting with, and helping train, several talented undergraduates, graduate students, and postdoctoral fellows, and has learned a great deal in many delightful conversations with professional colleagues (of whom Jack Simons, Michael Morse, and Benoit Soep deserve special recognition). On the occasion of his 60th birthday, Professor Breckenridge would like to dedicate this review article to his wife Julie, who has spent far too many hours waiting while he finished "working" at the dinner table.

Ne, Ar, Kr, and Xe. From a traditional inorganic chemistry point of view, in which $A^+(solvent)_1$ interactions have long been viewed as donor−acceptor (Lewis acid/Lewis base) interactions, such $A^+(Rg)_1$ bonds are thought of as weak, physical in nature, and quite irrelevant to real solvation by real polyatomic molecules. That view could well be short-sighted, we believe, since it is inherently biased toward the classical chemical ideas of bonding. Whatever one's view about $A^+\cdot(ligand)_1$ bonding, almost all chemists would agree that compared to the interaction of A^+ ions with such classic solvents as H_2O, NH_3, and organic molecules with Lewis-acid donor electron pairs, the rare-gas atoms are about as inert a solvent, chemically, as one can imagine.

However, even in a "Lewis-base" sense, is that *really* true? For example, the ionization potentials (see Table 1) of some of the inert gas atoms (roughly indicating the relative "instability" of the highest energy lone electron pair for donation to a given Lewis acid) are fairly low. Note especially, for example, that the prototypical chemical solvent molecule H_2O has a higher IP than Xe! This means, then, that examining $A^+\cdot Rg$ bonding is more generally relevant than might be thought by most chemists, especially if any trends in $A^+\cdot Rg$ bonding cannot be explained by "physical" attractive forces alone. The other side of the coin, of course, is that if $A^+\cdot Rg$ bonding *can* be explained by such physical forces, could some $A^+\cdot(H_2O)$ or $A^+\cdot(NH_3)$ "chemical" bonding *really* be almost entirely "physical" in nature?

Table 1. Ionization Potentials of Various Species[110]

species	IP (ev)
He	24.6
Ne	21.6
Ar	15.8
Kr	14.0
Xe	12.1
N_2	15.6
CO	14.0
H_2O	12.6
NH_3	10.2

Along such lines, the strong intermolecular interaction between two H_2O molecules can now be rationalized quite adequately without any significant "hydrogen-bonding" at all! Ab initio calculations, as well as models which are based only on long-range electrostatic and polarization attractive terms, are showing that hydrogen "*bonding*" may truly be a figment of chemist's imaginations, in that less than 10% of the attraction between two H_2O molecules is due to anything "special" (intermolecular charge transfer, say, or the "chemical" sharing of a proton between two O-atoms, the traditional chemical idea of a hydrogen bond[1]). Even further along these lines

(and perhaps stretching the point a bit to get the reader's attention), recent calculations[2] show that weak "hydrogen bonds" between C−H and O═C carbonyl groups may contribute significantly to protein folding; this type of bond is quite obviously not "hydrogen bonding" at all and can undoubtedly be explained totally by electrostatic, inductive, and dispersive attractive terms.

Similarly, Peyerimoff, in a very careful theoretical study,[3] has recently shown that the strong ("Lewis acid/base") binding of Li^+ to one H_2O molecule (~1.5 eV binding energy) involves essentially no charge transfer *at all*; the binding can be described as 73% electrostatic (charge/multipole) and 25% polarization (charge/induced-multipole), with only 2% charge transfer. (Let it be noted, however, that Peyerimoff's calculations for "true" Lewis-acid/Lewis-base complexes such as $H_3N{\cdot}BH_3$ indicated significant charge transfer, consistent with the classical ideas of "chemical" bonding, although "physical" polarization was *also* shown to be the major factor in H_3N/BH_3 attraction.[3])

The purpose of this review is to collect, present, and examine the extensive experimental and theoretical information now available for A^+·Rg diatomic ion interactions. We interpret data for several A^+·Rg ground and excited states (see below) using a model potential consisting of calculated (or estimated) attractive terms with dependence on A^+/Rg distances R ranging from $1/R^4$ (the significant charge/induced-dipole term) to $1/R^8$ and an Ae^{-bR} repulsive term derived empirically from experimental or ab initio data on bond energies D_e, bond distances R_e, and fundamental vibrational frequencies ω_e. It is found, in most cases, that such a "physical" model of bonding in A^+·Rg diatomic molecules is adequate, qualitatively reasonable, and quite useful in comparing (and understanding) the A^+/Rg interactions for a wide variety of such complexes.

II. Presentation of Data

Collected in Tables 2 and 3 are a comprehensive set of experimental and theoretical data[4−181] on bond energies D_e (cm^{-1}), bond lengths R_e (Å), and fundamental vibrational frequencies ω_e (cm^{-1}) for A^+·Rg ground-state and excited-state potential curves. Our recommended values for a given state are listed first, in ***bold***. Theoretical ab initio values are listed in parentheses, and experimental values which (in our opinion) are fairly uncertain are listed in brackets.

In this review, we discuss some of these data in the context of the "model-potential" analysis we have recently developed (building on earlier less complete or less general approaches[7,64]) to treat A^+/Rg "physical" bonding.[101,168,169] While there are obviously other ways to view the bonding, such as using molecular orbital or Lewis acid/base ideas (as discussed above), the physical model-potential approach is quantitative, general, and remarkably successful in rationalizing such bonding. We therefore leave to other authors any discussion of A^+·Rg bonding within the context of such qualitative bonding models.

III. Model-Potential Analysis for A^+·Rg States for Which A^+ Has No Permanent Quadrupole Moment

Theoretical and experimental investigators agree that the long-range $1/R^4$ ion/induced-dipole force is a major attractive force between A^+ ions and Rg atoms, especially at large internuclear distances R but also near the A^+·Rg bond-distance R_e, where the potential energy $V(R)$ minimizes. The electric field from the charge Z on the A^+ ion induces a dipole moment μ_{Rg} on a Rg atom of the following magnitude[1,7,64,145,146] (all the equations below are in atomic units)

$$\mu_{Rg} = \frac{+(Z){\cdot}(\alpha_{Rg})}{R^2} \tag{1}$$

where α_{Rg} is the dipole polarizability of the Rg atom. The induced dipole on the Rg atom interacts with the electric field from the charge Z on the A^+ ion, lowering the potential energy V (the factor of "$^1/_2$" results from the energy expenditure necessary to separate the charge on the Rg atom and *create* the induced dipole, the so-called "self-energy"[164,165]).

$$V(R) = \frac{-\,{}^1/_2(\mu_{\dot{R}g}){\cdot}(Z)}{R^2} \tag{2}$$

The net energy lowering, then, depends on Z^2, α_{Rg}, and R^{-4}

$$V(R) = \frac{-(Z^2)\,{\cdot}(\alpha_{Rg})}{2R^4} \tag{3}$$

This is the longest range (and usually the dominant) attractive term for A^+/Rg interactions. Many of the simplest A^+/Rg model potentials, in fact, have included only this single attractive (negative) term and a single two-parameter (positive) repulsion term, usually of the $+C_m/R^m$ or $+Ae^{-bR}$ form where C_m, m, A, and b are adjustable parameters

$$V(R) = \frac{-(Z^2)(\alpha_{Rg})}{2R^4} + Ae^{-bR}(\text{or} + C_m/R^m) \tag{4}$$

In this review, we have chosen to model the A^+/Rg data presented in Tables 2 and 3 with a somewhat more sophisticated potential function, with all possible attractive terms included out to $1/R^8$. For A^+ ions with no permanent quadrupole moment

$$V(R) = -\frac{\alpha_{Rg}{\cdot}(Z)^2}{2R^4} - \frac{C_6}{R^6} - \frac{\alpha_{RgQ}{\cdot}(Z)^2}{2R^6} + \frac{B_{Rg}{\cdot}(Z)^3}{2R^7} - \frac{C_8}{R^8} - \frac{\alpha_{RgO}{\cdot}(Z)^2}{2R^8} - \frac{\gamma(Z)^4}{24R^8} + Ae^{-bR} \tag{5}$$

where Z is the "effective" charge on the A^+ ion; α_{Rg}, α_{RgQ}, and α_{RgO} are the dipole, quadrupole, and octopole polarizabilities[1,7,64,121,122,145,146] of the Rg atom, B_{Rg} (*negative* value) is the higher-order "dipole−quadrupole" polarizability[64,121,146] of the Rg atom, γ is the-

Table 2. Bond Dissociation Energies D_e (cm^{-1}), Fundamental Vibrational Frequencies ω_e (cm^{-1}), and Bond Distances R_e (Å) for Ground States of A^+·Rg Complexes[a]

state of atomic ion A^+	molecular electronic state	A^+·He			A^+·Ne			A^+·Ar			A^+·Kr			A^+·Xe		
		D_e	ω_e	R_e	D_e	ω_e	R_e	D_e	ω_e	R_e	D_e	ω_e	R_e	D_e	ω_e	R_e
$Li^+(1s1s^1S_0)$	$^1\Sigma^+$	**(651)[177,178]**	**(276)[61,177−179]**	**(1.898)[179]**	**(1001)[5]**	**(231)[5,61]**	**(2.04)[5]**	**(2320)[8]**	**(268)[8,61]**	**(2.37)[8]**						
	(filled shell)	(649)[177]	(276)[61,177]	(1.897)[177]	(1005)[179]	(230)[179]	(2.04)[179]	(2368)[179]	(270)[179]	(2.364)[179]	(2859)[179]	(262)[179]	(2.52)[179]	(3569)[179]	(265)[179]	(2.72)[179]
		(653)[178]	(276)[61,178]	(1.894)[178]	(∼1050)[98]		(2.04)[98]	(2287)[9]	(262)[9]	(2.37)[9]	(2615)[13]	(256)[13]	(2.56)[13]	(2960)[20]	(245)[20]	(2.82)[20]
		(652)[16]	(263)[16,61]	(1.894)[16]	[920][59]		[2.11][59]	(2190)[10]	(263)[10]	(2.38)[10]	[3183][4]		[2.52][4]	[4434][4]		[2.51][4]
		(602)[144]		(1.92)[144]	[968][6]		[2.06][6]	(2040)[11]	(245)[11]	(2.42)[11]	[3710][59]		[2.45][59]	[4310][59]		[2.51][59]
		(581)[100]		(1.92)[100]	[1034][7]		[1.99][7]	(∼2000)[98]		(2.38)[98]						
		(546)[14]		(1.95)[14]				[2173][4]		[2.40][4]						
		(∼525)[97]		(2.06)[97]				[2520][59]		[2.42][59]						
		[596][76]		[1.96][76]				[2195][12]		[2.43][12]						
		[570][59]		[1.96][59]												
		[593][4]		[1.92][4]												
$Na^+(2p^6\ ^1S_0)$	$^1\Sigma^+$	**(329)[150]**	**(157)[61,150]**	**(2.33)[150]**	**(514)[150]**	**(107)[61,150]**	**(2.47)[150]**	**(1333)[150]**	**(125)[150]**	**(2.78)[150]**						
	(filled shell)	(329)[179]	(155)[179]	(2.324)[179]	(514)[179]	(107)[179]	(2.47)[179]	(1333)[179]	(125)[179]	(2.78)[179]	(1693)[179]	(118)[179]	(2.92)[179]	(2184)[179]	(119)[179]	(3.10)[179]
		(327)[15]	(151)[15,61]	(2.33)[15]	(508)[15]	(109)[15,61]	(2.47)[15]	(1306)[15]	(124)[15,61]	(2.79)[15]	[1778][18]		[2.91][18]	[2079][18]		[2.98][18]
		(∼290)[19]		(∼2.4)[19]	(508)[17]	(118)[17]	(2.48)[17]	(1310)[7]		(2.77)[7]	[1774][4]		[2.87][4]	[2089][4]		[3.11][4]
		(270)[17]	(129)[17]	(2.41)[17]	[520][4]		[2.49][4]	(1153)[17]	(110)[17]	(2.86)[17]				(1694)[20]	(105)[20]	(3.21)[20]
		[285][4]		[2.41][4]				[1504][4]		[2.70][4]						
$K^+(3p^6\ ^1S_0)$	$^1\Sigma^+$															
	(filled shell)	(177)[69]	(100)[69,61]	(2.85)[69]	(312)[179]	(69)[179]	(2.95)[179]	(830)[179]	(81)[179]	(3.23)[179]	(1075)[179]	(74)[179]	(3.37)[179]	(1378)[179]	(73)[179]	(3.56)[179]
		(178)[179]	(97)[179]	(2.85)[179]	[314][4]		[2.97][4]	[990][4]		[3.11][4]	[1135][4]		[3.30][4]	[1721][4]		[3.35][4]
		(171)[70]		(2.87)[70]	[292][7]		[2.97][7]	[763][7]		[3.27][7]				(903)[20]	(57)[20]	(3.77)[20]
		[164][4]		[2.90][4]												
		[147][7]		[2.91][7]												
$Rb^+(4p^6\ ^1S_0)$	$^1\Sigma^+$															
	(filled shell)	[142][4]		[3.10][4]	[263][4]		[3.19][4]	[652][4]		[3.49][4]	[926][4]		[3.54][4]	[1440][4]		[3.56][4]
Cs^+ $(5p^6\ ^1S_0)$	$^1\Sigma^+$															
	(filled shell)	[117][4]		[3.38][4]	[241][4]		[3.38][4]	[670][4]		[3.58][4]	[935][4]		[3.62][4]	[935][4]		[4.03][4]
$Be^+(2s\ ^2S_{1/2})$	$^2\Sigma^+$							**4500 ± 700*[23,24,89]**	**362.7[23]**	**2.086[23]**	**6500 ± 1000*[,25]**	**364[25]**	**2.220[25]**	**11,000 ± 2000*[,26]**	**367[26]**	
	($s\sigma$)	(124)[155]	(73)[155]	(2.96)[155]	(359)[155]	(68)[155]	(2.59)[155]	(∼3800)[98]		(2.10)[98]	[5,400][25,72]			[9,100][26,72]		
		(∼110)[97]		(3.13)[97]				4100 ± 200[23]								
								4500[89]								
								[3735][23,72]								
$Mg^+(3s\ ^2S_{1/2})$	$^2\Sigma^+$				**216 ± 100*[,106]**	**46*[,106]**	**315*[,106]**	**1290 ± 60[28]**	**100 ± 3*[,29]**	**2.81 ± 0.03*[,27]**	**1949 ± 100[30]**	**116*[,29]**	**∼2.80*[,66]**	**2910 ± 100[30]**	**124*[,29]**	**∼2.90*[,66]**
	($s\sigma$)				[117 ± 50][106]			1345[28,29]			2048[30,29]			4226[30,29]		
								1330 ± 165[29,30,74]			1932 ± 590[29,30,74]			3422 ± 1650[29,30,74]		
		(65)[156]	(44)[156]	(3.56)[156]	(179)[102]	(38.7)[102]	(3.25)[102]	(1088)[31]	(94)[31]	(2.85)[31]	(1923)[31]	(119)[31]	(2.89)[31]			
		(73)[17]		(3.56)[17]	(169)[17]	(33)[17]	(3.30)[17]	(1137)[17]	(92)[17]	(2.89)[17]						
$Ca^+(4s\ ^2S_{1/2})$	$^2\Sigma^+$				**115[153]**	**26*[,153]**	**3.70*[,153]**	**810 ± 60[32]**	**69 ± 2*[,33]**	**3.20 ± 0.15*[,62]**	**1283 ± 80[32]**	**77 ± 2*[,33,35]**	**3.30 ± 0.15*[,62]**	**1853 ± 100[32]**	**84 ± 2*[,33]**	**3.45 ± 0.15*[,62]**
	($s\sigma$)							735 ± 100[33]			1439[33]			2343[33]		
		(30)[34]		(4.4)[34]	(124)[34]		(4.0)[34]	890 ± 100[35]								
		(51)[90]		(4.1)[90]				(826)[85]	(73)[85]	(3.15)[85]	(1287)[85]	(68)[85]	(3.20)[85]			
					(90)[160]	(21)[160]	(3.87)[160]	(763)[160]	(65)[160]	(3.17)[160]						
$Sr^+(5s\ ^2S_{1/2})$	$^2\Sigma^+$					**19.5 ± 1.5[36]**			**50 ± 3[37]**			**52 ± 1[38]**			**54.6[181]**	
	($s\sigma$)				[77][36]			[827 ± 244][37]			[1231 ± 580][38]			[1974^{+435}_{-1200}][181]		
								(694)[81]	(39)[81]	(3.66)[81]						
$Ba^+(6s\ ^2S_{1/2})$	$^2\Sigma^+$							**850 ± 150***	**60*[,39]**	**3.36[39]**						
	($s\sigma$)							[680][39]	62[39]							
								[∼800][88]		[3.47][88]						

Table 2 (Continued)[a]

state of atomic ion A^+	molecular electronic state	A^+·He			A^+·Ne			A^+·Ar			A^+·Kr			A^+·Xe		
		D_e	ω_e	R_e	D_e	ω_e	R_e	D_e	ω_e	R_e	D_e	ω_e	R_e	D_e	ω_e	R_e
$Sc^+(3d4s\ ^3D)$	$^3\Delta$															
	$(d\delta)(s\sigma)$	(49)[17]	(31)[17]	(4.10)[17]	(121)[17]	(23)[17]	(3.69)[17]	(1202)[17]	(97)[17]	(2.91)[17]						
$Ti^+(3d^24s\ ^4F_{3/2})$	$^4\Phi$															
	$(d\pi)(d\delta)(s\sigma)$	(403)[117]	(315)[117]	(2.15)[117]	(532)[117]	(123)[117]	(2.43)[117]	(2420)[117]	(163)[117]	(2.65)[117]						
								(1903)[137]		(2.65)[137]						
$Zr^+(4d^25s\ ^4F_{3/2})$	$^4\Phi_{3/2}$							**∼2780**[131]		**∼2.70**[131]						
	$(d\pi)(d\delta)(s\sigma)$															
$V^+(3d^4\ ^5D)$	$^5\Sigma^+$							**∼3050**[103]	**165 ± 10***	**2.62 ± 0.02**[103]	**∼3890**[105]			**∼5350**[105]		
	$(d\pi)^2(d\delta)^2$	(1060)[17]	(320)[17]	(2.06)[17]	(700)[17]	(114)[17]	(2.51)[17]	(2600)[117]	(155)[117]	(2.65)[117]				[6680 ± 560][128]		
$Nb^+(4d^4\ ^5D_0)$	$^5\Sigma^+$							**∼3030**[132]		**∼2.67**[132]				**∼5900**[104]		
	$(d\pi)^2(d\delta)^2$															
$Cr^+(3d^5\ ^6S)$	$^6\Sigma^+$							**∼2400**[130]								
	$(d\sigma)(d\pi)^2(d\delta)^2$	437 ± 50[124,129]			532 ± 50[124,129]			∼2350[124]						[5700 ± 850][125]		
		[493 ± 158][129]			[665 ± 330][129]											
		(363)[117]	(160)[117]	(2.35)[117]	(419)[17]	(82)[17]	(2.69)[17]	(1928)[117]	(111)[117]	(2.70)[117]						
$Mn^+(3d^54s\ ^7S)$	$^7\Sigma^+$															
	$(d\sigma)(d\pi)^2(d\delta)^2(s\sigma)$	(81)[17]	(48)[17]	(3.49)[17]	(186)[17]	(35)[17]	(3.31)[17]	(1057)[17]	(76)[17]	(3.02)[17]						
$Fe^+(3d^64s\ ^6D)$[135]	$^6\Delta$[135]															
	$(d\sigma)(d\pi)^2(d\delta)^3(s\sigma)$	(113)[117]	(64)[117]	(3.27)[117]	(226)[17]	(41)[17]	(3.16)[17]	(1145)[117]	(75)[117]	(2.91)[117]				[4100 ± 525][134]		
								[1855 ± 160][142]						[3185 ± 500][126,127]		
														[3790 ± 650][133]		
								(1490)[135]	(98)[135]	(2.80)[135]	(2500)[135]	(110)[135]	(2.83)[135]	(3661)[135]	(114)[135]	(2.95)[135]
$Co^+(3d^8\ ^3F)$	$^3\Delta_3$							**∼4210**[104,138]	**205 ± 10***	**2.37 ± 0.01**[104,138]	**∼5600**[104]	**175 ± 10***	**2.43 ± 0.02**[104]	**∼8100**[104]		
	$(d\sigma)(d\pi)^4(d\delta)^3$	(1390)[117]	(350)[117]	(1.87)[117]	(920)[17]	(136)[17]	(2.35)[17]	(4030)[140]	(198)[140]	(2.36)[140]	(5092)[140]	(166)[140]	(2.48)[140]	(7021)[140]	(170)[140]	(2.60)[140]
								(3370)[117]	(192)[117]	(2.44)[117]				[6860 ± 600][141]		
$Ni^+(3d^9\ ^2D_{5/2})$	$^2\Sigma^+$							**4685 ± 25**[105]								
	$(d\sigma)(d\pi)^4(d\delta)^4$								[225 ± 50][105]							
		(1560)[17]	(376)[17]	(1.83)[17]	(1180)[17]	(165)[17]	(2.25)[17]	(3970)[17]	(192)[17]	(2.37)[17]						
								(3680)[136]		(2.42)[136]						
$Cu^+(3d^{10}\ ^1S_0)$	$^1\Sigma^+$															
	(filled shell)	(887)[17]	(271)[17]	(1.97)[17]	(774)[17]	(88)[17]	(2.37)[17]	(3270)[17]	(193)[17]	(2.37)[17]	(4682)[13]	(153)[13]	(2.46)[13]	(5100)[20]	(131)[20]	(2.63)[20]
								(3700)[82]	(175)[82]	(2.51)[82]						
$Ag^+(4d^{10}\ ^1S_0)$	$^1\Sigma^+$															
	(filled shell)							>2 500[152]			>2 900[152]			>3 900[152]		
														(3070)[20]	(102)[20]	(3.04)[20]
$Au^+(5d^{10}\ ^1S_0)$	$^1\Sigma^+$															
	(filled shell)	(214)[21]	(93)[21]	(2.75)[21]	(419)[21]	(71)[21]	(2.90)[21]	(2355)[21]	(123)[21]	(2.73)[21]	(4113)[21]	(120)[21]	(2.71)[21]	(7340)[21]	(129)[21]	(2.76)[21]
														(10,600)[22]	(149)[22]	(2.57)[22]
$Zn^+(4s\ ^2S_{1/2})$	$^2\Sigma^+$							**2085 ± 100**[101]	**∼117***[,48]	**∼2.65***[,48]						
	$(s\sigma)$															
$Cd^+(5s\ ^2S_{1/2})$	$^2\Sigma^+$							**∼1525***[,50]	**∼88***[,50]	**∼2.87***[,50]						
	$(s\sigma)$															
$Hg^+(6s\ ^2S_{1/2})$	$^2\Sigma^+$				**346**[45−47]	**57.8 ± 1.0**[45−47]	**2.98 ± 0.03**[45−47]	**1790 ± 100***[,41,43]	**99.0**[40]	**2.86 ± 0.01**[40]	**3150 ± 150***[,42,68]		**∼2.8***	**6020 ± 150***[,42,68]		**∼2.8***
	$(s\sigma)$							1810 ± 140[41,68]								
								1775[43]								
								[1630][40]								

Table 2 (Continued)[a]

state of atomic ion A^+	molecular electronic state	A^+·He			A^+·Ne			A^+·Ar			A^+·Kr			A^+·Xe		
		D_e	ω_e	R_e	D_e	ω_e	R_e	D_e	ω_e	R_e	D_e	ω_e	R_e	D_e	ω_e	R_e
$B^+(2s2s\ ^1S_0)$	$^1\Sigma^+$															
	(filled shell)	(∼180)[97]	(87)[97]	(2.91)[97]				(2150)[58]		(2.45)[58]						
		(∼190)[78]		(∼2.9)[78]				(2180)[93]		(2.49)[93]						
					(420)[98]		(2.52)[98]	(1960)[98]		(2.43)[98]						
		(140)[151]		(2.64)[151]	(1260)[151]		(2.45)[151]	(2520)[151]		(2.59)[151]	(4025)[151]		(2.64)[151]	(6475)[151]		(2.71)[151]
$Al^+(3s3s\ ^1S_0)$	$^1\Sigma^+$							**1025**[53]	**87***[54,107]	**3.10 ± 0.04***[55,107]	**1574**[53]	**94***[54]	**3.05***[55]			
	(filled shell)								$\Delta G_{1/2}$=82.2 ± 0.4[107]							
									[67][86]							
								(865)[87]	(76)[87]	(3.22)[87]						
$Ga^+(4s4s\ ^1S_0)$	$^1\Sigma^+$															
	(filled shell)							(584)[60]	(51)[60]	(3.37)[60]	(2100)[77]		(3.14)[77]			
$Tl^+(6s6s\ ^1S_0)$	$^1\Sigma^+$															
	(filled shell)				[∼400][84]		[∼2.8][84]	[∼1600][84]		[∼2.6][84]	[∼2200][84]		[∼2.8][84]			
$C^+(2s^22p\ ^2P)$	$^2\Pi$															
	(pπ)	(∼390)[97]		(2.41)[97]	(1050)[98]		(2.08)[98]	(7200)[98]		(2.09)[98]						
		(∼200)[92]		(2.27)[92]				(7450)[93]	(304)[93]	(2.04)[93]						
		(>200)[95]		(2.59)[95]				(9500)[80]	(485)[80]	(2.00)[80]						
				(2.5)[79]				[7600][80]	[417][80]	[2.00][80]						
$Si^+(3s^23p\ ^2P)$	$^2\Pi$															
	(pπ)			(3.2)[79]				(2076)[59]		(2.80)[59]						
$N^+(2s^22p^2\ ^3P)$	$^3\Sigma^-$															
	(pπ_{+1}pπ_{-1})	(∼1450)[97]		(1.75)[97]	(3790)[96]	(391)[96]	(1.75)[96]	(17,200)[93]		(1.86)[93]						
		(∼350)[83]		(2.12)[83]	(3220)[98]		(1.77)[98]	(17,050)[98]		(1.84)[98]						
		(∼600)[92]		(1.69)[92]												
$O^+(2s^22p^3\ ^4S)$	$^4\Sigma^-$															
	(pσpπ_{+1}pπ_{-1})	(∼280)[97]		(2.47)[97]	(420)[98]		(2.27)[98]	(3500)[98]		(2.29)[98]						
$F^+(2s^22p^4\ ^3P)$	$^3\Pi$															
	(pσpπ^3)	(∼490)[97]		(2.12)[97]	(1260)[98]		(1.96)[98]									
$Ne^+(2s^22p^5\ ^2P)$	$^2\Sigma^+$	**6410**[148]	**1308**[149]	**1.30**[149]												
	(pσpπ^4)															
$Ar^+(3s^23p^5\ ^2P_{3/2})$	$^2\Sigma^+$	**281.6**[108]	**120.3**[147]	**2.58**[147]												
	(pσpπ^4)	282.6[148]		2.57[108]												
		[262][147]														
$Kr^+(4s^24p^5\ ^2P_{3/2})$	$^2\Sigma^+$	**208**[143]		**2.87**[143]												
	(pσpπ^4)															

[a] Bold entries are our choices of "best" values for the parameters (an asterisk indicates a value which has been estimated by us). Theoretical ab initio values are in parentheses. Experimental values (or estimates from experimental information), which are relatively uncertain, we believe, are in brackets.

Table 3. Bond Dissociation Energies D_e (cm^{-1}), Fundamental Vibrational Frequencies ω_e (cm^{-1}), and Bond Distances R_e (Å) for Excited States of A^+·Rg Complexes[a]

state of atomic ion A^+	molecular electronic state	A^+·He			A^+·Ne			A^+·Ar			A^+·Kr			A^+·Xe		
		D_e	ω_e	R_e	D_e	ω_e	R_e	D_e	ω_e	R_e	D_e	ω_e	R_e	D_e	ω_e	R_e
$Be^+(2p\ ^2P_{1/2})$	$^2\Pi_{1/2}$							**11870 ± 1000*[,71,73]**	**582.98[71]**	**1.934[23,71]**	**14650 ± 1000*[,25,73]**	**554.47[25]**	**2.067[25]**	**20800 ± 2000*[,26,73]**	**545[26]**	
	(pπ)	(5845)[155]	(916)[155]	(1.38)[155]	(4119)[155]	(472)[155]	(1.72)[155]	[12,870][71,72]			[15,860][25,72]			[19,040][26,72]		
		(5460)[97]		(1.42)[97]				[11,470][23]								
$Be^+(2p\ ^2P_{3/2})$	$^2\Pi_{3/2}$							**11870 ± 1000*[,71,73]**	**582.98[71]**	**1.934[23,71]**	**14650 ± 1000*[,25,73]**	**554.47[25]**	**2.067[25]**	**20800 ± 2000*[,26,73]**	**545[26]**	
	(pπ)	(5845)[155]	(916)[155]	(1.38)[155]	(4119)[155]	(472)[155]	(1.72)[155]	[12,870][71,72]			[15,860][25,72]			[19,040][26,72]		
		(5460)[97]		(1.42)[97]				[11,470][23]								
$Mg^+(3p\ ^2P_{1/2})$	$^2\Pi_{1/2}$				**1964 ± 100*[,73,106]**	**219[106]**	**2.17 ± 0.06*[102,163]**	**5589*[,29,73]**	**272[29]**	**2.38 ± 0.06*[31,163]**	**7165*[29,73]**	**258[29]**	**2.45 ± 0.10*[,31]**	**9760*[,29,73]**	**258[29]**	**2.55 ± 0.15***
	(pπ)				1865[106]			5683[29,72]			7250[29,72]			11,168[29,72]		
		(2263)[156]	(468)[156]	(1.86)[156]	(1660)[102]	(204)[102]	(2.20)[102]	(5230)[31]	(265)[31]	(2.41)[31]	(7150)[31]	(255)[31]	(2.53)[31]			
$Mg^+(3p\ ^2P_{3/2})$	$^2\Pi_{3/2}$				**1923 ± 100*[,73,106]**	**219[106]**	**2.17 ± 0.06*[,102,163]**	**5548*[,29,73]**	**272[29]**	**2.38 ± 0.06*[,31,163]**	**7064*[,29,73]**	**256[29]**	**2.45 ± 0.10*[,31]**	**9485*[,29,73]**	**255[29]**	**2.55 ± 0.15***
	(pπ)				1830[106]			5618[29,72]			7221[29,72]			10,803[29,72]		
		(2263)[156]	(468)[156]	(1.86)[156]	(1660)[102]	(204)[102]	(2.20)[102]	(5230)[31]	(265)[31]	(2.41)[31]	(7150)[31]	(255)[31]	(2.53)[31]			
$Mg^+(3p\ ^2P_{1/2})$	$^2\Sigma^+$															
	(pσ)							(97)[162]		(5.2)[162]				(290)[162]		(4.8)[162]
$Ca^+(3d\ ^2D)$	$^2\Delta$															
	(dδ)	(140)[34]		(2.9)[34]	(299)[34]		(3.0)[34]	(1642)[85]	(~118)[85]	(2.94)[85]	(2040)[85]	(~106)[85]	(3.08)[85]			
$Ca^+(3d\ ^2D)$	$^2\Pi$															
	(dπ)	(189)[34]		(2.6)[34]	(231)[34]		(3.4)[34]	(1500)[85]	(~113)[85]	(2.97)[85]	(1957)[85]	(~106)[85]	(3.09)[85]			
$Ca^+(3d\ ^2D)$	$^2\Sigma^+$				**74 ± 5[153]**	**21.5[153]**	**~4.0*[,153]**	**418*[,35,73]**			**739*[,35,73]**					
	(dσ)	(13)[34]		(4.8)[34]	(73)[34]		(4.0)[34]	(436)[85]	(~40)[85]	(3.48)[85]	(792)[85]	(~53)	(3.40)[85]			
								[450][35]	[42][35]		[320][35]	[60][35]				
$Ca^+(4p\ ^2P_{1/2})$	$^2\Pi_{1/2}$				**870 ± 40[153]**	**134.5[153]**		**2971*[33,73]**	**165[33]**		**3854*[33,73]**	**149[33]**		**4551*[,33,73]**	**142[33]**	
	(pπ)	(710)[34]		(2.38)[34]	(535)[34]		(2.78)[34]	[2945][33,72]			[4173][33,72]			[4949][33,72]		
		(722)[90]		(2.43)[90]				(2888)[85]	(~163)[85]	(2.83)[85]	(3792)[85]	(~145)[85]	(2.96)[85]			
$Ca^+(4p\ ^2P_{3/2})$	$^2\Pi_{3/2}$				**945 ± 60[153]**	**131.7[153]**		**3037*[,33,73]**	**164[34]**		**3890*[,33,73]**	**149[34]**		**4,519*[,33,73]**	**139[34]**	
	(pπ)	(710)[34]		(2.38)[34]	(535)[34]		(2.78)[34]	[2,972][33,72]			[3,924][33,72]			[4,965][33,72]		
		(722)[90]		(2.43)[90]				(2888)[85]	(~163)[85]	(2.83)[85]	(3792)[85]	(~145)[85]	(2.96)[85]			
$Ca^+(4p\ ^2P_{3/2})$	$^2\Sigma^+$															
	(pσ)	(7.5)[34]		(7.0)[34]	(14)[34]		(6.3)[34]	(132)[85]		(5.29)[85]						
		(8.3)[90]		(6.1)[90]												
$Ca^+(5s\ ^2S)$	$^2\Sigma^+$															
	(sσ)	(1250)[34]		(2.3)[34]	(1000)[34]		(2.6)[34]									
$Ca^+(4d\ ^2D)$	$^2\Delta$															
	(dσ)	(800)[34]		(2.4)[34]	(1250)[34]		(2.6)[34]									
$Ca^+(4d\ ^2D)$	$^2\Pi$															
	(dπ)	(1200)[34]		(2.4)[34]	(850)[34]		(2.55)[34]									
$Sr^+(5p\ ^2P_{1/2})$	$^2\Pi_{1/2}$					**112 ± 4[36]**			**120.8 ± 0.5[37]**			**99.5 ± 0.5[38]**			**92.2[181]**	
	(pπ)				[558][36,72]			[2,190][37,72]			[2430][38,72]			[4023^{+290}_{-1300}][181]		
$Sr^+(5p\ ^2P_{3/2})$	$^2\Pi_{3/2}$					**100.2 ± 0.7[36]**			**122.0 ± 0.5[37]**			**100.0 ± 0.5[38]**			**97[181]**	
	(pπ)				[750][36,72]			[2330][37,72]			[2,500][38,72]			[4305^{+580}_{-110}][181]		
								(1970)[81]	(99)[81]	(3.17)[81]						
$Ba^+(6p\ ^2P_{1/2})$	$^2\Pi_{1/2}$							**~1600 ± 200*[,73]**	**96.6[39]**	**3.270[39]**						
	(pπ)							[1419][39]								
$Ba^+(6p\ ^2P_{3/2})$	$^2\Pi_{3/2}$							**~2100 ± 200*[,73]**	**102.0[39]**	**3.223[39]**						
	(pπ)							[1924][39]								

Table 3 (Continued)[a]

state of atomic ion A^+	molecular electronic state	A^+·He			A^+·Ne			A^+·Ar			A^+·Kr·Kr			A^+·Xe		
		D_e	ω_e	R_e	D_e	ω_e	R_e	D_e	ω_e	R_e	D_e	ω_e	R_e	D_e	ω_e	R_e
$Ti^+(3d^24s\ ^4F)$	$^4\Sigma^-$															
	$(d\delta)^2(s\sigma)$	(218)[117]	(227)[117]	(2.23)[117]	(387)[117]	(118)[117]	(2.50)[117]	(2049)[117]	(146)[117]	(2.68)[117]						
$Ti^+(3d^24s\ ^4F)$	$^4\Pi$															
	$(d\pi)(d\delta)(s\sigma)$	(57)[117]	(35)[117]	(3.91)[117]	(97)[117]	(40)[117]	(2.73)[117]	(1662)[117]	(125)[117]	(2.73)[117]						
$Ti^+(3d^24s\ ^4F)$	$^4\Delta$															
	$(d\sigma)(d\delta)(s\sigma)$	(75)[117]	(35)[117]	(3.79)[117]	(129)[117]	(27)[117]	(3.73)[117]	(678)[117]	(51)[117]	(3.39)[117]						
$Ti^+(3d^3\ ^4F)$	$^4\Delta$															
	$(d\Pi)^2(d\delta)$	(1032)[117]	(310)[117]	(2.12)[117]	(621)[117]	(135)[117]	(2.59)[117]	(2073)[117]	(135)[117]	(2.77)[117]						
$Ti^+(3d^3\ ^4F)$	$^4\Pi$															
	$(d\sigma)(d\pi)(d\delta)$	(121)[117]	(74)[117]	(3.18)[117]	(226)[117]	(56)[117]	(3.20)[117]	(976)[117]	(79)[117]	(3.22)[117]						
	+															
	$(d\pi)(d\delta)^2$															
$Ti^+(3d^3\ ^4F)$	$^4\Sigma^-$															
	$(d\sigma)(d\pi)^2$	(89)[117]	(60)[117]	(3.46)[117]	(169)[117]	(46)[117]	(3.42)[117]	(758)[117]	(60)[117]	(3.38)[117]						
$Ti^+(3d^3\ ^4F)$	$^4\Phi$															
	$(d\sigma)(d\pi)(d\delta)$	(96)[117]	(62)[117]	(3.40)[117]	(161)[117]	(62)[117]	(3.46)[117]	(694)[117]	(62)[117]	(3.47)[117]						
$Zr^+(4d^25s\ ^2G_{7/2})$	$(\Omega' = 5/2)$							**1207**[131]	**74.9**[131]	**3.02**[131]						
$V^+(3d^4\ ^5D)$	$^5\Delta$															
	$(d\sigma)(d\pi)^2(d\delta)$							(1799)[117]	(126)[117]	(2.65)[117]						
$V^+(3d^4\ ^5D)$	$^5\Pi$															
	$(d\sigma)(d\pi)(d\delta)^2$							(1758)[117]	(114)[117]	(2.73)[117]						
$V^+(3d^34s\ ^5F)$	$^5\Sigma^-$															
	$(d\sigma)(d\delta)^2(5\sigma)$							(718)[117]	(60)[117]	(3.27)[117]						
$V^+(3d^34s\ ^5F)$	$^5\Phi$															
	$(d\sigma)(d\pi)(d\delta)(s\sigma)$							(702)[117]	(57)[117]	(3.31)[117]						
$V^+(3d^34s\ ^5F)$	$^5\Delta$															
	$(d\pi)^2(d\delta)(s\sigma)$							(686)[117]	(56)[117]	(3.36)[117]						
$V^+(3d^34s\ ^5F)$	$^5\Pi$															
	$(d\pi)(d\delta)^2(s\sigma)$							(661)[117]	(54)[117]	(3.32)[117]						
$V^+(3d^34s\ ^5P_2)$	$^5\Pi_1$							**1406 ± 10**[103]	**90.4**[103]	**2.89 ± 0.02**[103]	**2098**[105]	**94.0**[105]		**3276**[105]	**107.9**[105]	
	$(d\pi)(d\delta)^2(s\sigma)$															
$Nb^+(4d^35s\ ^5P_2)$	$^5\Pi_1$													**3093**[104]	**85.2**[104]	
	$(d\pi)d\delta)^2(s\sigma)$															
$Cr^+(3d^44s\ ^6D)$	$^6\Sigma^+$															
	$(d\pi)^2(d\delta)^2(s\sigma)$	(97)[117]	(54)[117]	(3.47)[117]				(1460)[117]	(86)[117]	(2.87)[117]						
		[81 ± 14][129]			[367 ± 123][129]											
$Cr^+(3d^44s\ ^6D)$	$^6\Pi$															
	$(d\sigma)(d\pi)(d\delta)^2(s\sigma)$	(89)[117]	(54)[117]	(3.50)[117]				(1024)[117]	(65)[117]	(3.07)[117]						
$Cr^+(3d^44s\ ^6D)$	$^6\Delta$															
	$(d\sigma)(d\pi)^2(d\delta)(s\sigma)$	(97)[117]	(56)[117]	(3.44)[117]				(903)[117]	(64)[117]	(3.15)[117]						
$Fe^+(3d^64s\ ^6D)$	$^6\Pi$															
	$(d\sigma)(d\pi)^3(d\delta)^2(s\sigma)$	(113)[117]	(57)[117]	(3.35)[117]				(1040)[117]	(75)[117]	(2.97)[117]						
$Fe^+(3d^64s\ ^6D)$	$^6\Sigma^+$															
	$(d\sigma)^2(d\pi)^2(d\delta)^2(s\sigma)$	(105)[117]	(53)[117]	(3.33)[117]				(815)[117]	(63)[117]	(3.18)[117]						
$Fe^+(3d^7\ ^4F)$[135]	$^4\Phi$[135]															
	$(d\sigma)(d\pi)^3(d\delta)^3$	(1161)[117]	(341)[117]	(1.96)[117]				(2573)[117]	(150)[117]	(2.53)[117]						
$Fe^+(3d^7\ ^4F)$	$^4\Sigma^-$															
	$(d\sigma)(d\pi)^2(d\delta)^4$	(928)[117]	(229)[117]	(2.03)[117]				(2605)[117]	(153)[117]	(2.55)[117]						

Table 3 (Continued)[a]

state of atomic ion A^+	molecular electronic state	A^+·He			A^+·Ne			A^+·Ar			A^+·Kr			A^+·Xe		
		D_e	ω_e	R_e	D_e	ω_e	R_e	D_e	ω_e	R_e	D_e	ω_e	R_e	D_e	ω_e	R_e
$Fe^+(3d^7\ ^4F)$	$^4\Pi$															
	$(d\sigma)(d\pi)^3(d\delta)^3$	(669)[117]	(206)[117]	(2.11)[117]				(1879)[117]	(115)[117]	(2.63)[117]						
	+															
	$(d\sigma)^2(d\pi)^3(d\delta)^2$															
$Fe^+(3d^7\ ^4F)$	$^4\Delta$															
	$(d\sigma)^2(d\pi)^2(d\delta)^3$	(274)[117]	(95)[117]	(2.50)[117]				(2291)[117]	(145)[117]	(2.57)[117]						
								(2700)[135]	(157)[135]	(2.46)[135]	(4050)[135]	(149)[135]	(2.53)[135]	(5950)[135]	(159)[135]	(2.64)[135]
$Co^+(3d^8\ ^3F)$	$^3\Pi$															
	$(d\sigma)(d\pi)^3(d\delta)^4$	(710)[117]	(235)[117]	(2.08)[117]				(2896)[117]	(149)[117]	(2.49)[117]						
	+															
	$(d\sigma)^2(d\pi)^3(d\delta)^3$															
$Co^+(3d^8\ ^3F)$	$^3\Sigma^-$															
	$(d\sigma)^2(d\pi)^2(d\delta)^4$	(460)[117]	(154)[117]	(2.26)[117]				(2589)[117]	(144)[117]	(2.52)[117]						
$Co^+(3d^8\ ^3F)$	$^3\Phi$															
	$(d\sigma)^2(d\pi)^3(d\delta)^3$	(444)[117]	(145)[117]	(2.22)[117]				(2516)[117]	(139)[117]	(2.50)[117]						
$Co^+(3d^74s\ ^5F)$	$^5\Phi$															
	$(d\sigma)(d\pi)^3(d\delta)^3(s\sigma)$	[121 ± 19][129]			[424 ± 91][129]											
		(129)[117]	(57)[117]	(3.27)[117]				(1524)[117]	(97)[117]	(2.79)[117]						
$Co^+(3d^74s\ ^5F)$	$^5\Sigma^-$															
	$(d\sigma)(d\pi)^4(d\delta)^2(s\sigma)$	(129)[117]	(55)[117]	(3.24)[117]				(1436)[117]	(97)[117]	(2.81)[117]						
$Co^+(3d^74s\ ^5F)$	$^5\Pi$															
	$(d\sigma)^2(d\pi)^3(d\delta)^2(s\sigma)$	(121)[117]	(56)[117]	(3.26)[117]				(1299)[117]	(82)[117]	(2.88)[117]						
$Co^+(3d^74s\ ^5F)$	$^5\Delta$															
	$(d\sigma)^2(d\pi)^2(d\delta)^3(s\sigma)$	(129)[117]	(61)[117]	(3.32)[117]				(1153)[117]	(72)[117]	(2.98)[117]						
$Co^+(3d^74s\ ^3F_4)$	$^3\Phi_4$							**1563**[104]	**101**[104]	**2.80 ± 0.02**[104]	**2888**[104]	**114**[104]		**4862**[104]	**124**[104]	
	$(d\sigma)(d\pi)^3(d\delta)^3(s\sigma)$															
$Co^+(3d^74s\ ^3F_3)$	"B"													**4950**[104]	**125**[104]	
	$[^3\Delta_3(?)]$															
	$(d\sigma)(d\pi)^4(d\delta)^3$															
$Co^+(3d^74s\ ^3F_2)$	$^3\Pi_2$							**1593**[104]	**100**[104]	**2.79 ± 0.02**[104]	**2941**[104]	**117**[104]		**5214**[104]	**128**[104]	
	$(d\pi)^3(d\delta)^4(s\sigma)$															
$Co^+(3d^8\ ^1D_2)$	$^1\Delta_2$							**~3300**[104]		**2.44 ± 0.02**[104]	**~4700**[104]		**2.44 ± 0.02**[104]	**~7200**[104]		
	$(d\sigma)(d\pi)^4(d\delta)^3$															
	+															
	$(d\sigma)^2(d\pi)^2(d\delta)^4$															
$Co^+(3d^8\ ^1D_2)$	$[^1\Pi_1(?)]$							**2804**[104]	**161**[104]	**2.62 ± 0.02**[104]	**3966**[104]	**152**[104]		**6184**[104]	**169**[104]	
	$(d\sigma)(d\pi)^3(d\delta)^4$															
	+															
	$(d\sigma)^2(d\pi)^3(d\delta)^3$															
$Co^+(3d^8\ ^3P_2)$	$^3\Pi_2$							**2900**[104]	**170**[104]		**4078**[104]	**157**[104]		**6330**[104]	**161**[104]	
	$(d\sigma)(d\pi)^3(d\delta)^4$															
	+															
	$(d\sigma)^2(d\pi)^3(d\delta)^3$															
$Ni^+(3d^9\ ^2D)$	$^2\Delta$															
	$(d\sigma)^2(d\pi)^4(d\delta)^3$	(775)[17]	(253)[17]	(1.97)[17]	(613)[17]	(88)[17]	(2.47)[17]	(3230)[17]	(176)[17]	(2.38)[17]						
								(2760)[13]	(161)[13]	(2.39)[13]						
$Ni^+(3d^9\ ^2D)$	$^2\Pi$															
	$(d\sigma)^2(d\pi)^3(d\delta)^4$	(678)[17]	(208)[17]	(2.09)[17]				(2726)[13]	(165)[13]	(2.43)[13]						

Table 3 (Continued)[a]

state of atomic ion A^+	molecular electronic state	A^+·He			A^+·Ne			A^+·Ar			A^+·Kr			A^+·Xe		
		D_e	ω_e	R_e	D_e	ω_e	R_e	D_e	ω_e	R_e	D_e	ω_e	R_e	D_e	ω_e	R_e
$Ni^+(3d^84s\ ^4F)$	$^4\Delta$															
	$(d\sigma)(d\pi)^4(d\delta)^3(s\sigma)$	[126 ± 21][129]			[354 ± 70][129]											
		(152)[17]	(68)[17]	(3.20)[17]	(307)[17]	(48)[17]	(2.96)[17]	(1770)[17]	(109)[17]	(2.70)[17]						
$Ni^+(3d^84s\ ^4F_{7/2})$	"a"							**1926**[105]	**108**[105]							
$Ni^+(3d^84s\ ^4F_{7/2})$	"b"							**1872**[105]	**105**[105]							
$Ni^+(3d^84s\ ^4F_{5/2})$	"c"							**1786**[105]	**99.2**[105]							
$Hg^+(5d^96s^2\ ^2D_{5/2})$	$^2\Sigma^+$ (Ω=1/2)							**1859 ± 100***[40,73]	**104.5**[40]	**2.954**[40]						
	$(d\sigma)(d\pi)^4(d\delta)^4(s\sigma)^2$							[1820][40]								
$B^+(2s2p\ ^3P)$	$^3\Pi$															
	$(s\sigma p\pi)$	(1960)[97]		(1.45)[97]	(2560)[98]		(1.74)[98]	(12,300)[98]		(1.86)[98]						
					(2260)[100]	(~250)[100]	(1.88)[100]	(13,500)[100]	(~530)[100]	(1.92)[100]						
$B^+(2s2p\ ^1P)$	$^1\Pi$															
	$(s\sigma p\pi)$				(7180)[100]	(~620)[100]	(1.69)[100]									
$Al^+(3s3p\ ^1P)$	$^1\Sigma^+$							**1081**[107]	**90.9 ± 0.35**[107]	**3.28 ± 0.06**[107]						
	$(s\sigma p\sigma)$															
$Ga^+(4p4p\ ^3P)$	$^3\Sigma^-$															
	$(p\pi_{+1}, p\pi_{-1})$							(12,557)[60]	(285)[60]	(2.24)[60]						
$Si^+(3s^23p\ ^2P)$	$^2\Sigma^+$															
	$(p\sigma)$							(319)[59]		(3.82)[59]						
$O^+(2s^22p^3\ ^2D)$	$^2\Pi$															
	$(p\pi)^3$	(~3,000)[92]		(1.32)[92]	(2210)[98]		(1.56)[98]									
		(~5,000)[94]		(~1.2)[94]												
$F^+(2s^22p^4\ ^1D)$	$^1\Sigma^+$															
	$(p\pi)^4$	(16,600)[97]		(1.02)[97]	(13,900)[98]		(1.46)[98]									
$Ne^+(2s^22p^5\ ^2P_{1/2})$	$^2\Pi_{1/2}$			**2.3186**[149]												
	$(p\sigma^2p\pi^3)$	347[149]	$\Delta G_{1/2}$=129.69[149]													
		369[148]														
$Ar^+(3s^23p^5\ ^2P_{3/2})$	$^2\Pi_{3/2}$	**143.4**[108]		**2.98**[108]												
	$(p\sigma^2p\pi^3)$	154.1[148]		3.01[148]												
$Ar^+(3s^23p^5\ ^2P_{1/2})$	$^2\Pi_{1/2}$	**181.6**[108]		**2.87**[147]												
	$(p\sigma^2p\pi^3)$	185.4[148]		2.86[108]												
		[154][147]														
$Kr^+(4s^24p^5\ ^2P_{3/2})$	$^2\Pi_{3/2}$	**116**[143]		**3.20**[143]												
	$(p\sigma^2p\pi^3)$															
$Kr^+(4s^24p^5\ ^2P_{1/2})$	$^2\Pi_{1/2}$	**149**[143]		**3.06**[143]												
	$(p\sigma^2p\pi^3)$															

[a] Bold entries are our choices of "best" values for the parameters (an asterisk indicates a value which has been estimated by us). Theoretical ab initio values are in parentheses. Experimental values (or estimates from experimental information) which are relatively uncertain, we believe, are in brackets. (For configurations with contributions from two molecular orbital occupations, both MO occupations are listed.)

Table 4. Values for Model-Potential Calculations: Ground-State Species unless Indicated

species	α_d (Å^3)[a]	α_q (Å^5)[b]	N[c]	mass (amu)
He	0.205[110]	0.101[111]	1.434[111]	4.00
Ne	0.396[110]	0.27[111]	4.45[111]	20.2
Ar	1.64[110]	2.08[111]	5.90[111]	39.95
Kr	2.48[110]	3.97[111]	6.70[111]	83.8
Xe	4.04[110]	8.8[111]	7.79[111]	131.3
Li^+	0.029[113]	0.0047[113]	1.434[111]	6.94
Na^+	0.148[113]	0.070[113]	4.45[111]	23.00
Be^+	3.7[112]	2.20[112]	0.77[111]	9.012
$Mg^+(3s)$	5.5[44]	6.22[112]	0.98[111]	24.31
$Mg^+(3p\sigma)^h$	+3.4[44]	(+6)[e]	1.00[f]	24.31
$Mg^+(3p\pi)^h$	+4.4[44]	(+6)[e]	1.00[f]	24.31
Ca^+	11[112]	54[112]	1.05[111]	40.08
Ba^+	18[112]	200[112]	1.16[111]	137.3
Zn^+	2.8[139]	(4)[e]	6[114]	65.39
Cd^+	3.5[139]	(4.5)[e]	6.5[114]	112.41
$Hg^+(5d^{10}6s)$	2.7(± 0.2)[139]	(4)[e]	7[114]	201.97
$Hg^+(5d^96s^2)^h$	+5.4(± 0.4)[g]	(+6)[e]	7[114]	201.97
Al^+	4.0[115]	4.1[115]	1.94[111]	26.98
$V^+(3d^4)$	4.0[f]	(6)[e]	4[114]	50.94
$Co^+(3d^8)$	2.5[f]	(4)[e]	8[114]	58.93
$V^+(3d^34s)^h$	+6.2[d,110]	(+8)[e]	2[114]	50.94
$Co^+(3d^74s)^h$	+3.7[d,110]	(+5)[e]	4[114]	58.93
Cu^+	0.98[154] 0.89[116]	(1.5)[e]	10[114]	63.55
Ag^+	1.36[154] 1.18[116]	(2)[e]	10[114]	107.87
Au^+	1.75[154] 1.72[116]	(3)[e]	10[114]	196.97

[a] Dipole polarizability. [b] Quadrupole polarizability. [c] Effective number of "oscillator" electrons in the species, for the Slater−Kirkwood formula for calculating C_6.[1] [d] Our estimate (~50% of α_d for $3d^{n-1}4s^2$ neutral atom; this approximation works very well for Mg^+, Zn^+, Cd^+, Hg^+ [110,139]). [e] A guess! [f] Our estimate. [g] Our estimate (twice that of $Hg^+(5d^{10}6s)$). An approximate "ratio" estimate, assuming that the first 6s to 6p transitions carry *all* the oscillator strengths for both the $Hg^+(5d^{10}6s)$ ground state and the metastable $Hg^+(5d^96s^2)$ excited states, using *J*-state-weighted average energies, yields a consistent value of 5.2 Å^3 for the $Hg^+(5d^{10}6s^2)$ excited state. [h] Excited states.

higher-order "second dipole hyperpolarizability"[64,122,146] of the Rg atom, and C_6 and C_8 are *Z*-independent coefficients representing the first (random-dipole/induced-dipole) and second (random-dipole/induced-quadrupole, random-quadrupole/induced-dipole) terms in the dispersion[1,7,64,145,146] interaction. The higher-order *B* term is due to the quadrupole moment component induced on the Rg atom by the product of the electric field strength gradient and the electric field strength.[146] The higher-order γ term is due to the dipole moment component on the Rg atom induced by the electric field strength cubed.[146] The dispersion coefficients are calculated by (i) the Slater−Kirkwood approximation[1] for the C_6 coefficients and (ii) a similar approximation derived by Koutselos and Mason[123] for the C_8 coefficients.

The Ae^{-bR} "exponential" form for the repulsive term has been chosen because it is the expected mathematical dependence[65] of electron−electron exchange repulsion on R (at moderate distances R).

By differentiating this model equation twice, one can generate two more equations.[168] The resulting first-derivative equation (set to zero) locates the potential energy minimum, $-D_e$ (at R_e), and the resulting second-derivative equation describes the "curvature" of the potential (related to ω_e) at R_e. If the R_e, D_e, and ω_e values of the particular state of the diatomic ion are known or can be reliably estimated, then the three equations can be solved simultaneously to yield the effective charge Z and the two constants A and b which represent the repulsive term, Ae^{-bR}. The values of α_{Rg}, α_{RgQ}, α_{RgO}, B_{Rg}, and γ_{Rg} are all reasonably well-known[1,7,64,121−123,145,146] from experiment or ab initio calculations. Values of $\alpha_{(A^+)}$ (dipole polarizability of A^+) and $\alpha_{Q(A^+)}$ (quadrupole polarizability of A^+) are also required, however, to calculate the C_6 and C_8 coefficients,[1,123] and these values are usually less accurately known or must be qualitatively estimated. Values chosen for calculation of the terms in eq 5 are listed in Tables 4 and 5. [Note: We have not attempted to include so-called "damping" functions,[1,7,145,146,177] which are designed to allow for the effects of A^+/Rg electron cloud "interpenetration" at very short distances R; any "damping" of the attractive terms near R_e is therefore essentially empirically included in the values of the two-parameter Ae^{-bR} repulsive curves derived (as well as in the derived values of Z).]

Table 5. Values of Octopole Polarizabilities α_o, "Dipole−Dipole−Quadrupole" Polarizabilities *B*, and "Second Dipole Hyperpolarizabilities" γ for the Rg Atoms Which Were Used in the Model-Potential Calculations (e = unit charge in atomic units)

Rg	α_o (Å^7)[113]	B (e^{-1} Å^6)[121]	γ (e^{-2} Å^7)[122]
He	0.123	−0.144	0.501
Ne	0.397	−0.286	1.383
Ar	6.16	−3.07	13.6
Kr	16.35	−6.53	30.2
Xe	42.7	−15.57	80.0

A. Values of *Z*

Shown in Table 6 are the values of Z derived from such fits for several different types of A^+·Rg states for which fairly reliable R_e, D_e, and ω_e values are available. As can be seen, the values of Z (for the most part, but see section IV) resulting from the A^+·Rg fits are quite remarkably close to 1.00. [If the Ba^+·Ar, Au^+·Rg cases, which we discuss below, are excluded, $Z_{avg} = 1.02$.] The values of Z calculated from the fit of reliable R_e, D_e, and ω_e values for the states shown in Table 6, then, show (for a wide variety of ionic ground states) that when all types of "physical" attractive interactions are *properly* included, no substantial "extra" chemical Lewis-base-type interactions of Rg atoms with A^+ ion Lewis acids are required to describe the bonding.

B. The Ae^{-bR} Repulsive Curves

While most of the Z values derived from the three-parameter fits to the model potential are essentially the $Z = 1.0$ value expected, showing the general validity of this simple "physical" bonding model, it is also important to examine the repulsive curves Ae^{-bR} which are empirically derived from the model potentials for such cases. Again, these repulsive curves make good qualitative sense (we only consider

Table 6. Values of *A*, *b*, and *Z* in Eq 5, Calculated from the Values of R_e, D_e, and ω_e Listed (see Tables 2 and 3)

A^+·Rg state	R_e (Å)	D_e (cm^{-1})	ω_e (cm^{-1})	A (cm^{-1})	b ($Å^{-1}$)	Z (au)
			$A^+(1s^2)$·Rg and $A^+(np^6)$·Rg states			
$Li^+(1s^2)$·He[b]	1.896	651	276	5.57×10^6	4.734	1.04
$Li^+(1s^2)$·Ne[b]	2.04	1001	231	1.67×10^7	4.796	1.03
$Li^+(1s^2)$·Ar[b]	2.37	2320	268	2.73×10^7	3.883	1.04
$Na^+(2p^6)$·He[b]	2.33	329	157	1.58×10^7	4.767	1.03
$Na^+(2p^6)$·Ne[b]	2.47	514	107	3.43×10^7	4.649	1.02
$Na^+(2p^6)$·Ar[b]	2.78	1333	125	4.62×10^7	3.831	1.04
			$A^+(ns)$·Rg states			
$Be^+(2s)$·He[b]	2.96	124	73	1.50×10^6	3.119	1.04
$Be^+(2s)$·Ne[b]	2.59	359	68	1.77×10^6	2.973	1.10
$Be^+(2s)$·Ar[a]	2.086	4500 ± 700	362.7	8.75×10^7	4.333	0.87 ± 0.23
$Mg^+(3s)$·He[b]	3.56	65	44	1.97×10^6	2.928	1.04
$Mg^+(3s)$·Ne[a]	3.15	216 ± 100	46	3.02×10^6	2.955	1.09 ± 0.40
$Mg^+(3s)$·Ar[a]	2.81 ± 0.03	1290 ± 60	100	1.70×10^7	3.166	0.99 ± 0.06
$Mg^+(3s)$·Kr[a]	2.80 ± 0.08	1949 ± 100	116	3.29×10^7	3.256	0.95 ± 0.09
$Mg^+(3s)$·Xe[a]	2.90 ± 0.08	2910 ± 100	124	4.08×10^7	3.065	0.99 ± 0.09
$Ca^+(4s)$·Ne[a]	3.70 ± 0.05	115	26	2.05×10^6	2.548	1.05 ± 0.07
$Ca^+(4s)$·Ar[a]	$\sim 3.20 \pm 0.15$	810 ± 60	69	2.53×10^7	3.042	0.84 ± 0.20
$Ca^+(4s)$·Kr[a]	$\sim 3.30 \pm 0.15$	1283 ± 80	77	5.39×10^7	3.103	0.93 ± 0.20
$Ca^+(4s)$·Xe[a]	$\sim 3.45 \pm 0.15$	1853 ± 100	84	8.17×10^7	3.008	0.98 ± 0.20
$Ba^+(6s)$·Ar[a]	3.36	(680)	60			(0.23)
	3.36	$\sim 850 \pm 150$?	60	4.57×10^7	3.032	$(\sim 0.7 \pm 0.3)$
$Zn^+(4s)$·Ar[a]	2.65 ± 0.05	2085 ± 100	~ 117	4.58×10^7	3.595	1.01 ± 0.12
$Cd^+(5s)$·Ar[a]	2.87 ± 0.05	1525 ± 100	~ 88	3.96×10^7	3.419	1.00 ± 0.12
$Hg^+(6s)$·Ne[a]	2.98 ± 0.03	346	57.8	2.56×10^7	3.776	1.02 ± 0.07
$Hg^+(6s)$·Ar[a]	2.86 ± 0.01	1790 ± 100	99.0	1.01×10^8	3.801	1.05 ± 0.09
$V^+(3d^34s)$·Ar[a]	2.89 ± 0.02	1406	90.4	2.68×10^7	3.240	1.01 ± 0.09
$Co^+(3d^7\ 4s)$·Ar[a]	2.80 ± 0.02	1563	101	4.04×10^7	3.485	0.96 ± 0.09
			$A^+(ns^2)$·Rg states			
$Al^+(3s^2)$·Ar[a]	3.10 ± 0.04	1025	87	1.90×10^7	3.095	1.08 ± 0.10
$Al^+(3s^2)$·Kr[a]	3.05 ± 0.05	1574	94	2.52×10^7	3.050	1.04 ± 0.10
$Hg^+(5d^96s^2)$·Ar[a]	2.954	1859 ± 100	104.5	1.96×10^8	3.907	1.02 ± 0.10
			$A^+(3d^n)$·Rg states			
$V^+(3d^4)$·Ar[b]	2.65	2600	155	1.27×10^8	3.973	1.02
$Co^+(3d^8)$·Ar[a]	2.37 ± 0.02	4210	205	1.57×10^8	4.252	1.02 ± 0.10
$Co^+(3d^8)$·Ar[b]	2.36	4030	198	1.36×10^8	4.207	0.99
$Co^+(3d^8)$·Kr[b]	2.48	5092	166	1.25×10^8	3.854	1.09
$Co^+(3d^8)$·Xe[b]	2.60	7021	170	1.64×10^8	3.655	1.11
			$A^+(nd^{10})$·Rg states			
$Cu^+(3d^{10})$·Xe[b]	2.63	5100	131	7.83×10^7	3.464	1.09
$Ag^+(4d^{10})$·Xe[b]	3.04	3070	102	6.94×10^8	4.137	0.97
$Au^+(5d^{10})$·He[b]	2.75	214	93	4.72×10^6	3.558	1.06
$Au^+(5d^{10})$·Ne[b]	2.90	419	71	9.70×10^7	4.357	1.04
$Au^+(5d^{10})$·Ar[b]	2.73	2355	123	1.90×10^8	4.150	1.11
$Au^+(5d^{10})$·Kr[b]	2.71	4113	120	2.52×10^8	4.046	1.19
$Au^+(5d^{10})$·Xe[b]	2.76	7340	129	2.79×10^8	3.749	1.32
$Au^+(5d^{10})$·Xe[b,c]	2.57[c]	10600[c]	149[c]	2.10×10^8	3.655	1.43

[a] Experimental (or experimental estimate from neutral Rydberg states). [b] Ab initio calculations. [c] Larger basis sets.

the Ae^{-bR} curves for the cases in which $Z \approx 1.00 \pm 0.11$).

1. Variation with "Size" of Rg Atom for the Same A^+ State

Shown in Figures 1−5 are a series of repulsive curves Ae^{-bR} derived from the model-potential analysis of selected reliable data in Tables 2 and 3 (see Table 6). These curves follow the expected qualitative trend, since the repulsion sets in at increasingly larger R as the "size" of the outer-shell electron cloud on the Rg atom increases. In fact, these curves follow remarkably well the pattern of estimated "hard-sphere" diameters[65] of the Rg atoms: 2.59, 2.73, 3.42, 3.62, and 4.14 Å for He, Ne, Ar, Kr, and Xe, respectively.

2. Variation with "Size" of A^+ State for the Same Rg Atom (Same Type of Outer-Shell Electronic Configuration for A^+)

In Figure 6 parts a and b, the expected increase in repulsion with "size" as the principle quantum number of the A^+ ion increases (Li^+Ar, Na^+Ar and the Be^+Ne, Mg^+Ne, Ca^+Ne series) is also observed.

In Figure 6c, the variation of the repulsive curves of A^+·Ar ions with $A^+(3d^n4s)$ outer-shell configurations is shown. As expected, because of the general decrease in size of the 4s outer-shell electron cloud across the first transition period,[158] the curves become less and less repulsive in the $V^+(3d^34s)$·Ar, $Co^+(3d^74s)$·Ar, $Zn^+(3d^{10}4s)$·Ar series. Note also, in comparing Figures 2 and 6c, that $Zn^+(4s)$ is even smaller than $Mg^+(3s)$, consistent with the very large bond strength and very short bond length of Zn^+·Ar

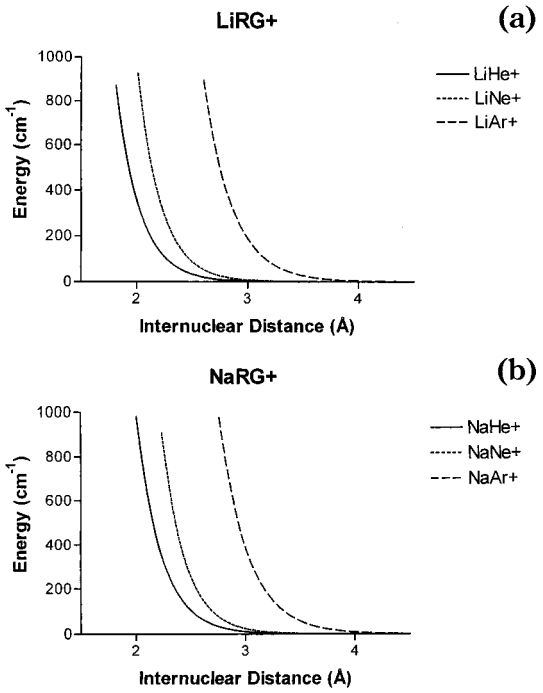

Figure 1. Plots of the repulsive curves Ae^{-bR} (see Table 6) for the same A^+ ground state, with varying Rg atoms: (a) Li^+Rg and (b) Na^+Rg.

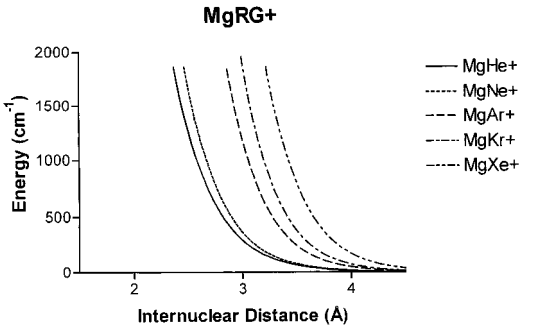

Figure 2. Plots of the repulsive curves Ae^{-bR} (see Table 6) for the same A^+ ground state, with varying Rg atoms: Mg^+Rg.

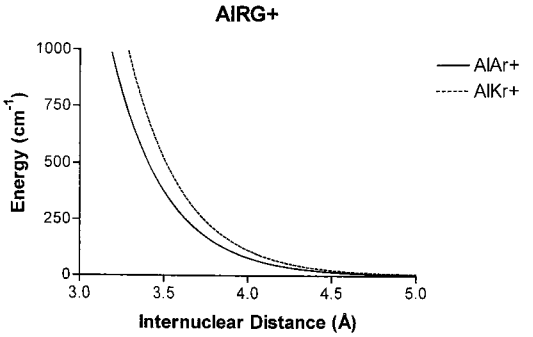

Figure 3. Plots of the repulsive curves Ae^{-bR} (see Table 6) for the same A^+ ground state, with varying Rg atoms: Al^+Rg.

(see Table 2), due to the first transition period orbital contraction.

3. Variation of Repulsion with Different Outer-Shell Electronic Configurations of A+, for a Given Rg Atom

Shown in Figure 7 are the differences in repulsive curves for $Li^+(1s^2)$·Rg versus $Be^+(2s)$·Rg ions. As

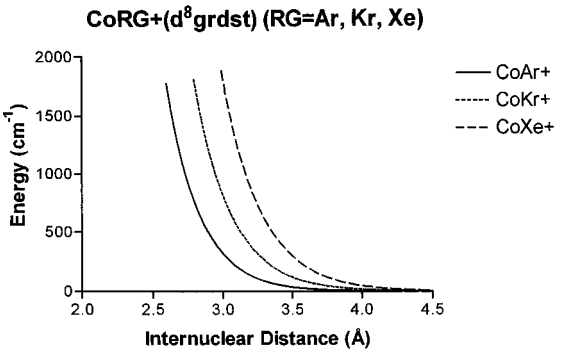

Figure 4. Plots of the repulsive curves Ae^{-bR} (see Table 6) for the same A^+ ground state, with varying Rg atoms: Co^+Rg.

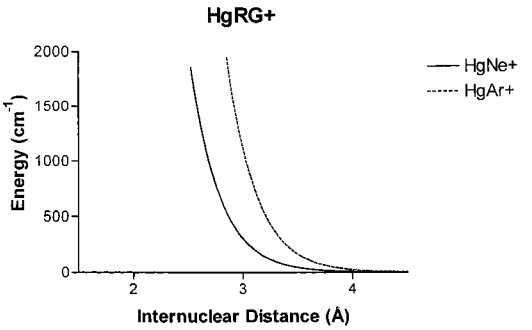

Figure 5. Plots of the repulsive curves Ae^{-bR} (see Table 6) for the same A^+ ground state, with varying Rg atoms: Hg^+Rg.

expected, the $1s^2$ electron cloud is much smaller than the 2s cloud, leading to much less repulsion. However, the *difference* in calculated repulsive curves for $Li^+(1s^2)$·Rg versus $Be^+(2s)$·Rg appears to *decrease* in the order He, Ne. This will be discussed again below, but it appears that as the Rg polarizability increases, there is more and more to gain by extending the attractive terms to smaller distances R than there is to lose by "back-polarization" (s−p hybridization) of the $Be^+(2s)$ electron cloud to minimize repulsion. Such "back-polarization" is very costly for the small, filled-shell $Li^+(1s^2)$ electron cloud and essentially does not occur.

The same kinds of trends are seen (Figure 8) for the repulsive curves of $Na^+(2p^6)$·Rg versus $Mg^+(3s)$·Rg ions. In the $Mg^+(3s)$·Ar case, Bauschlicher and co-workers[180] demonstrated the "back-polarization" of the $Mg^+(3s)$ electron cloud at smaller R values near R_e by plotting wave function contours. Surprisingly at first, the $Al^+(3s^2)$·Ar repulsion is slightly greater than that of $Mg^+(3s)$, even though the $Al^+(3s^2)$ electron cloud should be somewhat smaller than that of the $Mg^+(3s)$ electron cloud, due to the normal increase in effective nuclear charge. This observation may also be related to the ease of "back-polarization" (s → p promotion energy necessary for s−p hybridization), to avoid repulsion, of the single 3s electron on Mg^+ versus the less-polarizable filled-shell *pair* of 3s electrons on Al^+.

In Figure 9, again as expected, repulsion is much less for $A^+(3d^n)$·Ar versus $A^+(3d^{n-1}4s)$·Ar ions, due to the much smaller size of the 3d versus the 4s electron clouds.

Table 7. Variations of Calculated Z Values When Progressively Adding $1/R^7$, $1/R^8$ Terms to Eq 5 (R_e, ω_e, and D_e values listed in Table 6)

state	$1/R^4$,$1/R^6$ (only)	+	$1/R^7$	+	$1/R^8$ (α_{RgO})	+	$1/R^8$ (γ)	+	$1/R^8$ (C_8)	absolute uncertainty in Z
$Li^+(1s^2)Ne^b$	1.06		1.04		1.04		1.03		1.03	
$Na^+(2p^6)Ar^b$	1.07		1.05		1.04		1.04		1.04	
$Mg^+(3s)Ar^a$	1.09		1.08		1.07		1.06		0.99	±0.06
$Ca^+(4s)\cdot Ar^a$	1.01		1.00		0.99		0.99		0.84	±0.20

[a] Experimental estimate. [b] Ab initio calculation.

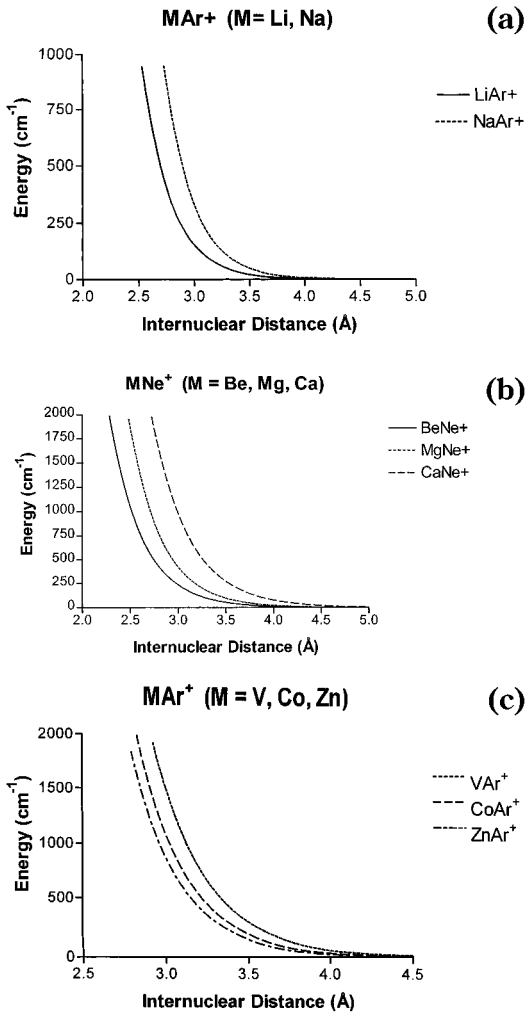

Figure 6. Plots of Ae^{-bR} repulsive curves (see Table 6) for $A^+\cdot Rg$ states which have the same type of outer-shell electronic configuration: (a) $Li^+(1s^2)\cdot Ar$ and $Na^+(2p^6)\cdot Ar$, (b) $Be^+(2s)\cdot Ne$, $Mg^+(3s)\cdot Ne$, and $Ca^+(4s)\cdot Ne$, (c) V^+Ar, Co^+Ar, and Zn^+Ar (all states have one 4s outer-shell electron.).

C. Effects on the Derived *Z*, *A*, *b* Values of Adding the Various "Higher" Attractive Terms in Eq 5

Our original model calculations[101] included only the attractive terms in eq 5 with power dependencies R^{-4} and R^{-6}, which were found (in many cases) to reproduce the R_e, D_e, and ω_e values with "reasonable" values of *Z*. Addition of the R^{-7}, R^{-8} terms in eq 5 provides marginal improvements in the *Z* values (e.g., derived *Z* values which are then slightly closer to 1.00 for $A^+\cdot Rg$ ions). Here we illustrate the effects of adding such terms on the values of Z and on the repulsive curves Ae^{-bR}.

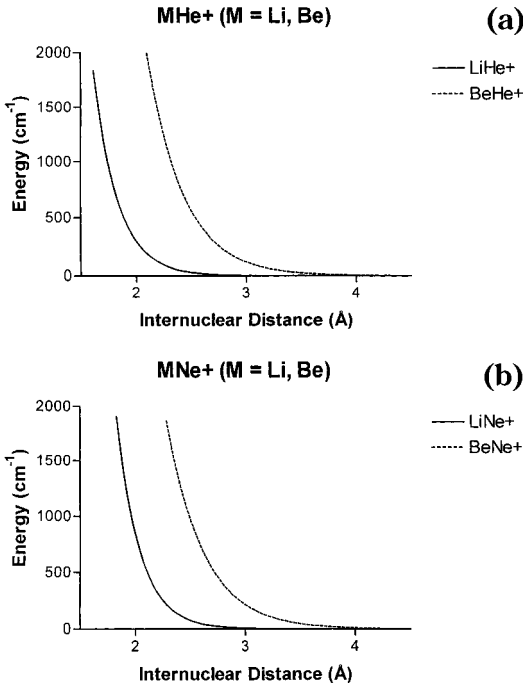

Figure 7. Plots of Ae^{-bR} repulsive curves for $A^+\cdot Rg$ states with the same Rg atom but for A^+ states which differ in their outer-shell electronic configurations. [$Li^+(1s^2)$, $Be^+(2s)$]: (a) Li^+He, Be^+He, (b) Li^+Ne, Be^+Ne.

1. Z Values

Shown in Table 7 are the values of *Z* obtained with the progressive addition of the various R^{-7}, R^{-8} terms for several representative cases. The R^{-7} term provides a 2−3% improvement in the *Z* values for most of the cases examined. The various R^{-8} terms also tended (usually) to improve the *Z* values but by varying amounts depending on the A^+ ion outer-shell electronic structure. For A^+ ions with small, "tight" outer-shell electron clouds, the effects on the *Z* values of adding all the R^{-8} terms were essentially negligible. However, for ions such as $Mg^+(3s)$, which have a large, diffuse outer-shell electron cloud (and thus large C_6 and C_8 "dispersion" attractive terms), the C_8/R^8 "dispersion" term decreased the calculated *Z* values substantially. In fact, the effect of the C_8/R^8 terms for such cases may be *too* great at R_e due to our total neglect of "damping" terms in the potential, which are designed to progressively "shut-down" the long-range attractions as the electron clouds of A^+ and Rg begin to interpenetrate (this "damping" sets in at progressively larger *R* values, as *n* increases, for R^{-n} attraction terms).[1,145,146]

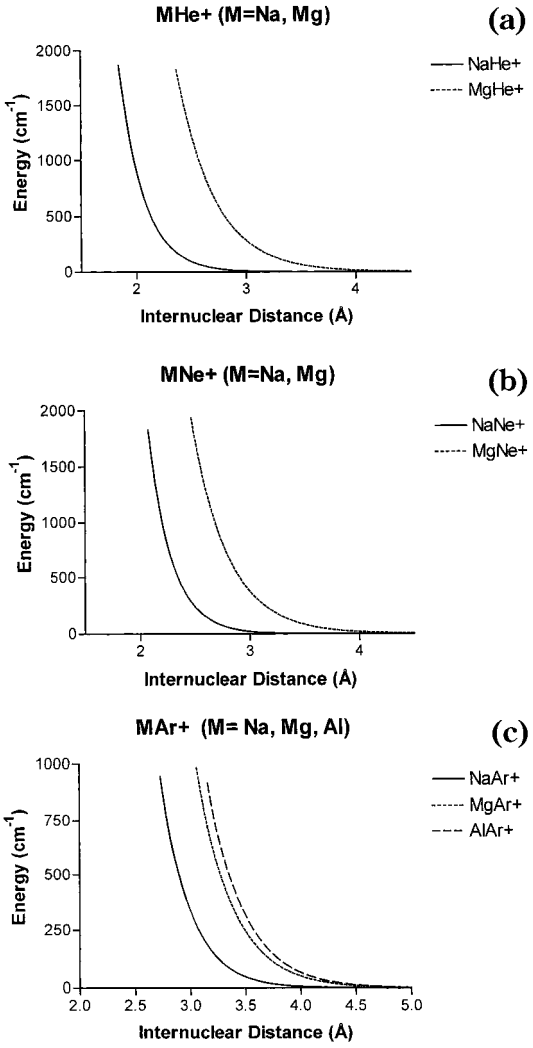

Figure 8. Plots of Ae^{-bR} repulsive curves for A^+·Rg states with the same Rg atom but for A^+ states which differ in their outer-shell electronic configurations. [$Na^+(2p^6)$, $Mg^+(3s)$, $Al^+(3s^2)$], (a) Na^+He, Mg^+He, (b) Na^+Ne, Mg^+Ne, (c) Na^+Ar, Mg^+Ar, Al^+Ar.

2. Repulsive Curves Ae^{-bR}

As observed in Figure 10, progressive addition of the $1/R^7$ and $1/R^8$ attractive Na^+Ar terms (not surprisingly) causes the Ae^{-bR} curves to become increasingly repulsive in nature but only slightly. (Note, however, that this does not *necessarily* have to be true if the addition of an attractive term *lowers* the value of Z appreciably.) Similar effects are observed for the Mg^+Ar case (Figure 11), *except* for the C_8 dispersive term, which leads to a derived Ae^{-bR} term which is *much* more repulsive. As discussed above, the "effective" magnitude of the $^{-}C_8/R^8$ term at R_e may be too high, however, for ions with large outer-shell electron clouds due to our neglect of "damping" of long-range attraction as A^+ and Rg charge clouds interpenetrate. This is consistent with the *greater* percent decrease in Z by the C_8 term for the Ca^+Ar ion, since the dipole and quadrupole polarizabilities of the Ca^+ ion are large.

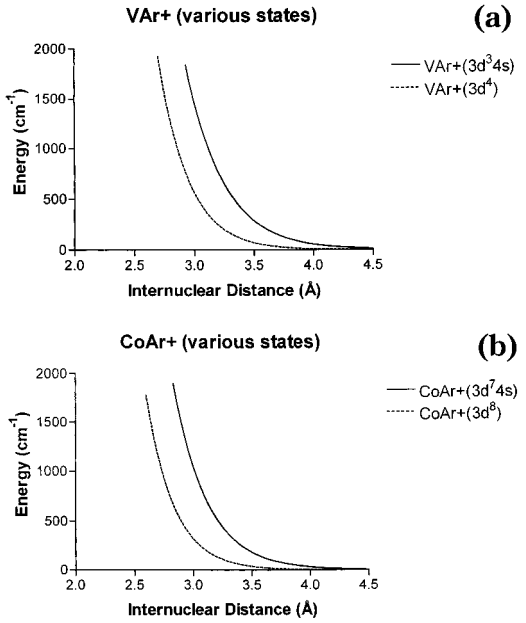

Figure 9. Plots of Ae^{-bR} repulsive curves for A^+·Rg states with the same Rg atom but for A^+ states which differ in their outer-shell electronic configurations. (a) $V^+(3d^4)$, $V^+(3d^34s)$, (b) $Co^+(3d^8)$, $Co^+(3d^74s)$.

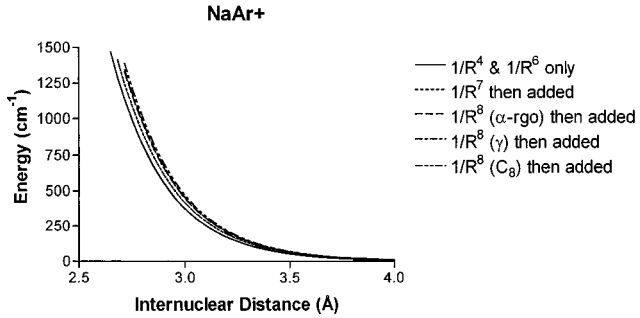

Figure 10. Plots of Ae^{-bR} curves for Na^+Ar which result from progressively adding attractive terms to eq 5. See Table 7.

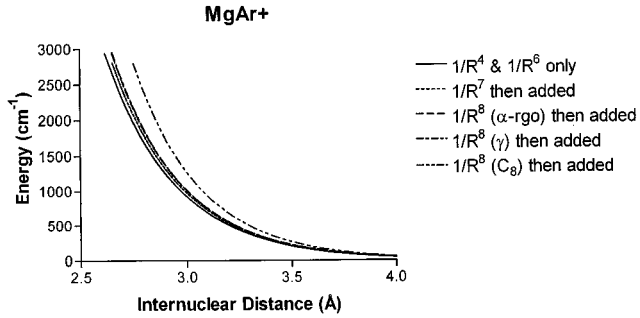

Figure 11. Plots of Ae^{-bR} curves for Mg^+Ar which result from progressively adding attractive terms to eq 5. See Table 7.

D. Detailed Comparison of Na^+Ar and Mg^+Ar Ground States

Our model-potential analysis has revealed differences in the importance of the various attractive (and the repulsive) terms in eq 5 for A^+·Rg complexes. Here we compare in detail (as an interesting example) the differences in the physical bonding in the Mg^+Ar and Na^+Ar ground states. From Table 2 it is seen that the D_e values (1333, 1290 cm^{-1}) and R_e

Table 8. Comparison of the Contributions of the Various Terms in Eq 5 for Na^+Ar versus Mg^+Ar at R_e for Each Ion

	Na^+Ar ($Z = 1.04$)		Mg^+Ar ($Z = 0.99$)	
terms	E (cm^{-1})	% total attraction	E (cm^{-1})	% total attraction
$1/R^4$ (ion/induced-dipole)	−1715	71	−1500	41
$1/R^6$ (ion/induced-quadrupole)	−281	12	−241	7
$1/R^6$ (C_6)	−95	4	−814	22
$1/R^7$	−155	6	−125	3.5
$1/R^8$ (ion/induced-octopole)	−107	4	−90	3
$1/R^8$ (γ)	−18	1	−17	0.5
$1/R^8$ (C_8)	−51	2	−829	23
total attraction	−2422	100	−3616	100
Ae^{-bR} (repulsion)	+1089	45	+2326	64
net	−1333	55	−1290	36

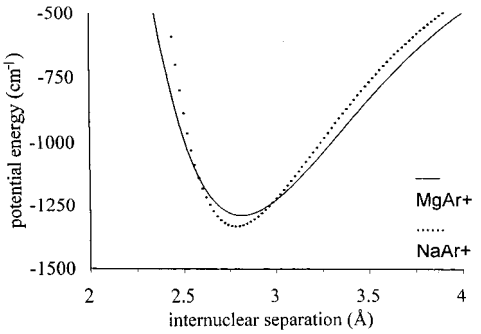

Figure 12. Plots of the derived potential curves for Na^+Ar and Mg^+Ar.

values (2.78, 2.81 Å) for the two species are remarkably similar, despite the *completely* different outer-shell electronic character of Na^+ and Mg^+. The $Mg^+(3s)$ ion has a large, polarizable ($\alpha_d = 5.5$ Å^3) outer-shell 3s electron, while the $Na^+(2p^6)$ ion has a tiny (and very unpolarizable ($\alpha_d = 0.148$ Å^3)) $2p^6$ outer shell, so it is at first glance surprising that their bond lengths and bond strengths are so similar. Note, however, that their vibrational frequencies, ω_e, are quite different (125 vs 100 cm^{-1}), indicating that the "shapes" of the two potential curves are very different near R_e. In Figure 12 we plot the two potential curves derived from the best-fit Z, b, and A values for eq 5.

We now examine the values of each of the terms in eq 5, at R_e, for Na^+Ar and Mg^+Ar. Shown in Table 8 are the absolute energies (and percentages of total attraction energies) at R_e for each attractive term in eq 5 for the two complexes. While the dominant term for Na^+Ar, as expected, is the R^{-4} ion/induced-dipole term (71%), the ion/induced-quadrupole and ion/induced-octupole terms (total of 16%) and the R^{-7} higher-order term (6%) add significantly to the attraction at R_e. However, because of the very small polarizability of the $Na^+(2p^6)$ ion, the C_6 and C_8 terms contribute a minor amount (total of 6%) to the attraction at R_e. At R_e, the total attraction is −2422 cm^{-1} and the repulsion is +1089 cm^{-1}, leading to a D_e of 1333 cm^{-1}. Thus, the repulsion is ∼45% of the attraction at R_e.

A completely different picture emerges for the Mg^+Ar ion. The absolute values of all the Z-dependent terms discussed above are qualitatively similar to those for Na^+Ar since the derived Z values and the experimental R_e values are similar for the two ions. However, because the dipole and quadrupole polarizabilities of the large $Mg^+(3s)$ ion are so much greater, the C_6 and C_8 terms add a huge attractive energy at R_e, about −1650 cm^{-1} total. This extra attraction must be matched approximately by a simultaneous increase in repulsion, since the D_e values of the two ions are similar. This makes sense, of course, given the much larger repulsive "size" of the $Mg^+(3s)$ ion versus the $Na^+(2p^6)$ ion.

As seen in Table 8, the "dominant" $1/R^4$ term for Mg^+Ar now actually contributes only 41% to the bonding, while the sum of the C_6, C_8 dispersion terms contribute 45%. The true effect (particularly due to the C_8 term contribution) is probably less because of our neglect of "damping" terms, but the much greater dispersive attraction must certainly be the major reason that $Mg^+\cdot Ar$ is as strongly bound as Na^+Ar. The extra attraction allows the Ar atom to move closer, at the expense of extra repulsion (and/or the cost of "back-polarization" of the $Mg^+(3s)$ orbital to minimize such repulsion). The total attraction at R_e is −3616 cm^{-1} (large), but the repulsion is +2326 cm^{-1} (large), leading to a D_e of 1290 cm^{-1}. The percentage of repulsion versus attraction, ∼64%, is thus much higher than that for the Na^+Ar case. This is expected since the Mg^+Ar repulsive potential is "softer" than the more "hard-sphere"-like Na^+Ar repulsive potential (see Figures 8c and 12). Also, the effective attractive R^{-n} dependence at R_e for Na^+Ar is only $n \approx 4$, while for Mg^+Ar it is probably closer to $n = 6$. [The smaller the *difference* in n and n' values for an "effective" $-C_n/R^n$ attractive term and an "effective" $+C_{n'}/R^{n'}$ repulsive term, for example, the greater the "% repulsion" at R_e, which is the value of R where $dV(R)/dR$ changes sign; a completely "hard-sphere" potential where $n' = \infty$, for example, would result in essentially "0%" repulsion at R_e or at least at an R which is *just* larger (by dR) than R_e.] These considerations explain the higher vibrational frequency of Na^+Ar versus Mg^+Ar (125 cm^{-1} versus 100 cm^{-1}), since the "stiffer" Na^+Ar repulsion on the inner wall (combined with less net *attraction* on the outer wall due to the much smaller C_6/R^6 and C_8/R^8 terms) causes a narrower potential curve near R_e (see Figure 12).

E. General Comparison of Na^+Rg and Mg^+Rg Ground States

A more general comparison of Mg^+Rg versus Na^+Rg states (see Table 2) shows the general importance of the C_6, C_8 dispersion terms and the "back-polarization" (to avoid repulsion) in the Mg^+Rg states. The

Table 9. Comparison of the Contributions of the Various Terms in Eqs 5, 7, 9, and 10 for $Hg^+(5d^{10}6s)$·Ar versus $Hg^+(5d^96s^2)$·Ar at R_e for Each Ion

	$Hg^+(5d^{10}6s)$·Ar ($Z = 1.05$; $R_e = 2.86$ Å)		$Hg^+(5d^96s^2)$·Ar ($Z = 0.98$; $R_e = 2.954$ Å)	
terms	E (cm^{-1})	% total attraction	E (cm^{-1})	% total attraction
$1/R^4$ (ion/induced-dipole)	−1585	42	−1197	31
$1/R^6$ (ion/induced-quadrupole)	−259	7	−174	5
$1/R^6$ (C_6)	−923	25	−1216	31
$1/R^7$	−134	3.5	−85	2
$1/R^8$ (ion/induced-octopole)	−90	2	−59	1.5
$1/R^8$ (γ)	−18	0.5	−10	0.3
$1/R^8$ (C_8)	−754	20	−878	23
$1/R^6$ (eq 7)	0	0	−164	4
$1/R^6$ (eq 9)	0	0	−41	1
$1/R^8$ (eq 10)	0	0	−6	0.2
$1/R^8$ (eq 13)	0	0	−52	1
total attraction	−3763	100	−3882	100
Ae^{-bR} (repulsion)	+1973	52	+2023	52
net	−1790	48	−1859	48

Na^+Rg states show steadily increasing D_e values *and* R_e values in the series He, Ne, Ar, Kr, Xe, which is what would normally be expected for a "hard" $Na^+(2p^6)$ ion core and the increasing polarizability of Rg atoms with size. (See the Wright series of very recent high-level ab initio values[179] in Table 2.)

In contrast, the D_e value for Mg^+He is much less than, and the R_e value much greater than, the D_e, R_e values for Na^+He. The attractive energy gained by back-polarization in the Mg^+He case is apparently not sufficient to off-set the expense of s−p hybridization, given the low polarizability of the He atom. As the polarizability of the Rg atom rises, energy gains in $1/R^4$, $1/R^6$, $1/R^8$ attractive terms increasingly outweigh the expense of s−p hybridization to minimize repulsion, and the D_e values for Mg^+Rg states rise much more rapidly with Rg size than in the Na^+Rg series. At the same time (see Figure 6a−c), the *relative* difference in the effective Ae^{-bR} repulsive terms for Mg^+Rg versus Na^+Rg drops slightly as Rg size increases, presumably because of the increasing "back-polarization" in the Mg^+Rg states. Thus, the Mg^+Rg R_e values *drop* rapidly, then go through a shallow minimum at Rg·Ar in the series He, Ne, Ar, Kr, Xe (3.56, 3.15, 2.81, ∼2.8, ∼2.9 Å). [Very similar trends (Table 2) are observed for the analogous Be^+Rg and Ca^+Rg states.] Note that the result is that Na^+Xe is less bound ($D_e = 2184$) than Mg^+Xe ($D_e = 2910$), with an R_e value which is greater (3.10 versus ∼2.9 Å).

F. Detailed Comparison of the $Hg^+(5d^{10}6s)$·Ar Ground State and the $Hg^+(5d^96s^2)$·Ar First Excited State

The R_e and ω_e values for the $Hg^+(5d^{10}6s\ ^2S)$·Ar[$^2\Sigma^+$] ground state and the $Hg^+(5d^96s^2\ ^2D_{5/2})$·Ar[$^2\Sigma^+$] excited state ($\Omega'' = {}^1/_2$, $\Omega' = {}^1/_2$, in the more appropriate notation of Hund's case (c))[40] were determined very early (1972) in a high-resolution emission study by Bridge[40] (with theoretical help by Hougen[156]). The difference in the D_e values for the two states is also accurately known from the $v_{0,0}$ band-origin, ω_e and $\omega_e x_e$ values for both upper and lower states, and the energy difference between the $Hg^+(6s\ ^2S)$ and $Hg^+(5d^96s^2\ ^2D_{5/2})$ atomic asymptotes: the excited $Hg^+(5d^96s^2)$·Ar state is slightly more bound than the $Hg^+(6s\ ^2S)$·Ar ground state but only by about 70 cm^{-1}. Until we recently performed our model-potential analyses of these two states, this had puzzled us for several years, even to the point of our questioning the spectroscopic assignments and analysis of Bridge and Hougen. For example, why is the excited state more bound than the ground state, even though the bond length of the excited state (2.95 Å) is almost 0.1 Å *larger* than that of the ground state (2.86 Å)?

It turns out that the answer is closely related to the main difference in the bonding of the Mg^+Ar versus the Na^+Ar ground states discussed above: differences in dispersive attraction. Because of two (consistent) direct photoionization threshold measurements of the $Hg^+(6s)$·Ar bond energy ($D_e = 1790 \pm 100$ cm^{-1}), the relative (and absolute) D_e of the excited state is also accurately established: 1859 ± 100 cm^{-1}. Shown in Table 9 is a comparison (similar to Table 8 for Mg^+Ar and Na^+Ar) indicating the contributions of the various attractive terms and the repulsive term to the bond energies for the ground and excited state of Hg^+Ar at R_e for each ion. As can be seen from Table 9, at the R_e value for each state the dispersive (C_6, C_8) terms for the $Hg^+(5d^96s^2)$·Ar state account for ∼55% of the attractive energy, compared to ∼45% for the $Hg^+(5d^{10}6s)$·Ar ground state, even though its R_e value is ∼0.1 Å greater.

Because of the larger dipole polarizability for the $Hg^+(5d^96s^2)$ ion versus the $Hg^+(5d^{10}6s)$ ion, due to the presence of two (versus one) polarizable 6s electrons, the C_6/R^6 and C_8/R^8 terms are larger for the $Hg^+(5d^96s^2)$ ion, while of course all the other (inductive) *attractive* terms are identical for the same effective Z value. The attractive energy, at a given R value, is therefore greater for the $Hg^+(5d^96s^2)$·Ar state than the $Hg^+(5d^{10}6s)$·Ar state. However, the two 6s electrons also cause more Ae^{-bR} *repulsion* for the $Hg(5d^96s^2)$·Ar state, as shown in Figure 13. The net result is that the potential minimum occurs at a larger R, 2.954 Å, for the $Hg(5d^96s^2)$·Ar state but with a substantial D_e value of 1859 cm^{-1} due to the greater attraction. The result for the $Hg^+(5d^{10}6s)$·Ar state is that a lower value of R is reached before the potential

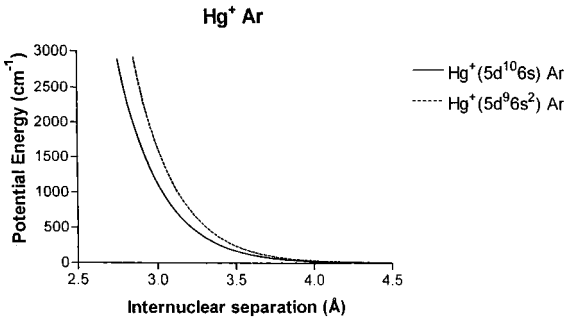

Figure 13. Plots of Ae^{-bR} curves for the $Hg^+(6s)$·Ar ground state and the $Hg^+(5d^96s^2)$·Ar excited state.

minimum occurs, 2.86 Å, because there is less *repulsion*. The D_e value is similar (1790 cm^{-1}), however, because there is also less *attraction*.

One final point can be made concerning an experimental observation in the Bridge spectroscopic study[40] of the Hg^+Ar molecular transitions. The weak atomic transition $Hg^+(5d^96s^2\ ^2D_{5/2}) \leftarrow Hg^+(5d^{10}6s\ ^2S_{1/2})$ shows large isotope shifts for the even isotopes (which can have no hyperfine splitting). These nuclear "volume" shifts[40] can be large (several tenths of a wavenumber) for heavy elements for transitions involving s electrons, which can penetrate to the nucleus and thus (incredibly!) are quite sensitive to small variations in the *size* of different isotopic nuclei. Bridge observed, when using natural mercury (he also performed measurements with 98% pure ^{202}Hg, to simplify the spectra), that *exactly* the same "volume" isotopic shift pattern as in the Hg^+ atomic spectra was observed for the sharp band heads in the Hg^+Ar spectra. This indicates that the "Hg^+" moieties in the Hg^+Ar molecular states are very similar to the asymptotic atomic Hg^+ states. There is therefore no major charge transfer in the $Hg^+(6s)Ar$ ground state, since this would surely increase the total Hg(6s) electron density at the nucleus, changing the isotopic shifts. This observation is thus quite consistent with our view that no true Lewis-acid/Lewis-base charge donation occurs in these A^+·Rg ions.

IV. The Few A^+·Rg States in Table 6 for Which the Derived "Effective" Z Value Is Different from 1.0 ± 0.2

A. Ba^+·Ar States

The R_e and ω_e values for the $Ba^+(6s)$·$Ar[^2\Sigma^+]$ ground states and the "pure-π" $Ba^+(6p\pi)$·$Ar[^2\Pi_{3/2}]$ state are quite accurately known from the cw dye-laser-induced fluorescence and dispersed fluorescence study of the $A^2\Pi_\Omega \leftarrow X^2\Sigma^+$ transitions by Panov, Williamson, and Miller.[39] However, their estimated value of D_e'' (and thus of $D_e'[^2\Pi_{3/2}]$) is uncertain, we believe. It is based on an "RKR" extrapolation of their derived ground-state potential curve; however, they only measured B_o'', and an *estimated* α_e'' value was used to construct the RKR curve. Since the Birge−Sponer plot of the ground state $\Delta G_{1/2}''$ values is *unusually* nonlinear, this may have been a particularly dangerous thing to do. In fact, in contrast to the analogous Mg^+Ar and Ca^+Ar ground states, we derive an unreasonably low value of $Z = 0.23$ (see Table 6) when we use their estimated value of $D_e' = 680\ cm^{-1}$. We believe that the true value of D_e' is probably about 850 cm^{-1}, which gives a more reasonable (but still low) value of $Z \approx 0.8$ for Ba^+Ar. As discussed above, the slightly lower Z values for Ca^+Ar (and Ba^+Ar?) could be due to our neglect of "damping" due to electron-cloud interpenetrations; the C_8 value is large for Ba^+Ar because of the large α_q value for the Ba^+ ion (=200 $Å^5$). However, in any case, a better experimental estimate of D_e' for the Ba^+Rg ion is certainly needed. [The relative ease of s−dσ hybridization may also reduce repulsion in Ba^+Ar, since the $Ba^+(5d\ ^2D)$ state is only ~5000 cm^{-1} higher than the $Ba^+(6s\ ^2S)$ ground state, as compared to ~14 000 cm^{-1} for the analogous $Ca^+(4d\ ^2D)$ state, so that $Ba^+(6s\ ^2S)$ could be as strongly bound as $Ca^+(4s\ ^2S)$·Ar. This is also consistent with the fairly short bond distance for $Ba^+(6s\ ^2S)$·Ar, 3.36 Å, compared to our estimate of 3.2 ± 0.15 Å for $Ca^+(4s\ ^2S)$·Ar, despite the fact that the Ba^+ ion is much larger than the Ca^+ ion.]

B. Au^+Xe Ground State

There are as yet no experimental estimates of R_e, ω_e, or D_e values for this state of which we are aware. However, relativistic ab initio calculations of Pyykko and co-workers predict very high bond energies and very short bond lengths for Au^+Xe. Their "best" calculation[22] yields $D_e'' = 10\ 600\ cm^{-1}$, $R_e'' = 2.57$ Å. Our model-potential analysis yields an unreasonably high value of $Z = 1.43$ to rationalize their D_e'', ω_e'', and R_e'' values. (Values of Z for their ab initio data for Au^+He, Au^+Ne yield normal values of $Z = 1.06$, 1.04, while for Au^+Ar and Au^+Kr, $Z = 1.11$, 1.19, values which are a bit too high.) It would be comforting to have an experimental spectroscopic or photoionization threshold confirmation of the high ab initio bond energy (given the difficulties inherent in ab initio calculations of a molecule with two heavy atoms), but it appears at this stage that Au^+Xe is the most likely M^+·Rg ground-state case yet reported in which the Rg atom could be exhibiting partial "σ-donor" Lewis base character. [Note, however (Table 6), that the analogous Cu^+Xe and Ag^+Xe complexes have "normal" values of Z, 1.09 and 0.97, respectively.]

The recent, unexpected preparation[170] of the $AuXe_4^{+2}$ "complex ion" is consistent with the Xe atom functioning as a Lewis-base electron donor to the Lewis-acid Au^{2+} ion. Such "chemistry" is more likely for the Au^{2+} ion than the Au^+ ion, of course, but this observation is certainly consistent with at least some chemical interaction in the Au^+·Xe diatomic ion.[170] The "Au^{2+}·Xe" bond lengths in the $AuXe_4^{2+}$ complex were determined (from X-ray diffraction)[170] to be only ~2.74 Å but still substantially longer than the Pyykko ab initio value of 2.57 Å for Au^+Xe. This is partially due to steric hindrince, we believe, since the Xe−Xe distances in the square planar $AuXe_4^{2+}$ complex are 3.88 Å compared to the Xe−Xe "hard-sphere" distance of ~4.1 Å.[65] (The bond distance of the Xe_2 van der Waals dimer is 4.36 Å.[99]) The Mulliken population analysis from ab initio calculations[170] also indicates that most of the positive charge resides on

the Xe atoms, with each Xe having a charge of 0.44 ± 0.03 au and the Au ion a charge of only +0.24 ± 0.11 au (Mulliken populations were not reported for the highest-level Pyykko Au^+Xe calculations, but for an earlier calculation,[21] the Xe atom was found to have +0.39 au of the positive charge according to Mulliken analysis but only +0.17 au of the positive charge according to natural bond order analysis, so the Mulliken numbers may be an overestimation of σ-donor character.)

Buckingham and Read[64] claim that their model-potential analysis of the first (lower-level) Pyykko ab initio results on Au^+Xe successfully rationalizes the bond energy, $D_e = 7340\ cm^{-1}$, at the calculated bond length, $R_e = 2.76$ Å, with a fixed $Z = 1.00$ and that there are therefore no "chemical" interactions in Au^+·Xe bonding. However, (i) they use a $+C_n/R^n$ repulsive term and are only able to get agreement for completely unphysical values of $n \approx 19$! Such a steep repulsive potential is necessary because they cannot otherwise account for enough attractive energy to rationalize the $V(R)$ minimum for a more reasonable repulsive potential of $n \approx 9-12$. (ii) They also make no attempt to account for the calculated *shape* of the potential at R_e (i.e., the calculated value of $\omega_e = 129\ cm^{-1}$), and their "fit" potentials lead to ω_e values much too large, due to the steep repulsion on the inner walls. (iii) If our model-potential results are any indication (see Table 7), their analysis would have even more difficulty rationalizing the higher-level[22] Pyykko calculations. Again, reliable experimental information on the Au^+Xe ion would be highly desirable.

C. Other Possible Cases

Because of the lack of reliable D_e, ω_e, and R_e information (often ω_e or R_e is not known accurately) or A^+ physical properties such as the polarizabilities, quadrupole moments, etc., the model-potential analysis has not been applied to every A^+/Rg state in Tables 2 and 3. It is possible, then, that future analysis, when sufficient reliable information becomes available, will reveal other cases where purely "physical" bonding ideas fail to describe a strong A^+/Rg bonding situation.

V. Model-Potential Analysis for A^+·Rg States for Which A^+ Has a Permanent Quadrupole Moment

A. $A^+(p\pi)$·Rg States

It has been known for some time that the first excited states of Mg^+·Rg complexes, $Mg^+(3p\pi)$·Rg[$^2\Pi$], are much more strongly bound and have much shorter bond lengths than their $Mg^+(3s)$·Ar[$^2\Sigma^+$] ground-state analogues[29,31,102,106,156] (see Table 10). We suggest that this is due to several effects.

1. Permanent Quadrupole Interaction Terms

The $Mg^+(3p\ ^2P_J)$ excited atomic state has a large (negative) quadrupole moment ($Q_{zz} = -1.59$ e·Å^2, where e is the unit charge, in atomic units)[44] due to the excited Mg(3p) electron cloud (−/++/− in character, similar to that of the CO_2 molecule, where $Q_{zz} = -0.93$ e·Å^2).[146]

Table 10. Comparison of D_e and R_e Values of the $Mg^+(3s)$·Rg($^2\Sigma^+$) Ground States and the $Mg^+(3p\pi)$·Rg($^2\Pi_{3/2}$) Excited States (see Tables 3 and 4)

	$^2\Sigma^+$		$^2\Pi_{3/2}$	
	D_e (cm^{-1})	R_e (Å)	D_e (cm^{-1})	R_e (Å)
Mg^+He[b]	65	3.56	2263	1.86
Mg^+Ne[a]	216	3.15	1923	2.17
Mg^+Ar[a]	1290	2.81	5548	2.38
Mg^+Kr[a]	1949	2.80	7064	2.45
Mg^+Xe[a]	2910	2.90	9485	2.55

[a] Experimental values or experimental estimates. [b] Ab initio calculations.

(a) When this 3p orbital is aligned in a "π" fashion, perpendicular to the A^+·Rg bond axis, the quadrupole moment can interact favorably with the substantial −/+ dipole moment induced on the Rg atom by the A^+ effective charge Z (eq 1).[1,39,146] The potential energy expression for this interaction is[1,146]

$$V(R)_{\mu,Q} = -\,{}^3/_2\left(\frac{\mu_{Rg}\cdot Q_{A^+}}{R^4}\right) \qquad (6)$$

where μ_{Rg} (positive value) is the (charge-induced) dipole, from eq 1, on the Rg atom and Q_{A^+} (positive value for $Mg^+(3p\pi)$ of +0.795 e·Å^2; negative value for $Mg^+(3p\sigma)$ of −1.59 e·Å^2, for example) is the permanent quadrupole moment tensor component of A^+ *along* the internuclear axis [see Appendix I; in the particular case of pπ alignment, $Q_{A^+} = Q_{xx} = Q_{yy} = -{}^1/_2 Q_{zz}$]. Note also that the expression in eq 6 is 50% smaller than that for the interaction of a permanent quadrupole with a permanent dipole[146] to allow for the "self-energy" necessary to create the induced dipole.[164,165] Thus, using eq 1

$$V(R)_{\mu,Q} = \frac{-\,{}^3/_2(Z)(\alpha_{Rg})(Q_{A^+})}{R^6} \qquad (7)$$

and this R^{-6} term must be added to eq 5.

There are also three other terms which must be added to eq 5 to account for all attraction terms (out to $1/R^8$) due to the permanent quadrupole moment of A^+. (b) There is an *additional substantial* dipole moment component induced on the Rg atom by the permanent quadrupole moment tensor component of A^+ along the bond axis.[146,166]

$$\mu_{Rg(Q)} = \frac{+3(Q_{A^+})(\alpha_{Rg})}{R^4} \qquad (8)$$

This quadrupole-induced dipole-moment component interacts with the *charge* Z on the A^+ atom[1,146] (eq 2).

$$V(R)_{Z,Q_{id}} = \frac{-\,{}^3/_2(Q_{A^+})(\alpha_{Rg})(Z)}{R^6} \qquad (9)$$

(Note that this $1/R^6$ term essentially *doubles* the potential energy term due to eq 7.) The quadrupole-induced dipole component, $\mu_{Rg(Q)}$, also interacts with

Table 11. Values of *Z* Calculated for the $Mg^+(3p\pi)\cdot Rg$ ($^2\Pi_{3/2}$) Excited States Using Eq 5 Only or Eq 5 with the Progressively Added "Permanent Quadrupole Moment" Attraction Terms of Eqs 7, 9, 10, and 13: $\alpha_d(Mg^+(3p\pi)) = 4.44$ Å^3;[44] $\alpha_q(Mg^+(3p\pi)) = 6$ Å^5 (estimated); Q_{A^+} for $Mg^+(3p\pi)$: +0.795 e·Å^2,[44] where e is the atomic unit of charge (see Appendix I); $N = 1$

Rg	R_e (Å)	D_e (cm^{-1})	ω_e (cm^{-1})	*Z* (au) [eq 5]	*Z* (au) [eq 7 term added to eq 5]	*Z* (au) [eqs 7 and 10 terms added to eq 5]	*Z* (au) [eqs 7, 9, and 10 terms added to eq 5]	*Z* (au) [eqs 7, 9, 10, and 13 terms added to eq 5]	absolute uncertainty in *Z*
He[b]	1.86	2263	468	1.48	1.31	1.27	1.14	1.11	
Ne[a]	2.17 ± 0.06	1923	220	1.38	1.20	1.17	1.07	1.05	±0.15
Ar[a]	2.38 ± 0.06	5548	272	1.40	1.32	1.30	1.22	1.19	±0.20
Kr[a]	2.45 ± 0.10	7064	256	1.37	1.30	1.28	1.21	1.18	±0.25

[a] Experimental estimates. [b] Ab initio calculation.

the permanent quadrupole moment tensor component of A^+ (this is the "permanent-quadrupole/induced-dipole" induction interaction (ref 146, p 90, eq 2.213), which is present even when $Z = 0$)[146,166] (see eq 6) and is always attractive

$$V(R) = \frac{-{}^9/_2(Q_{A^+})^2(\alpha_{Rg})}{R^8} \qquad (10)$$

Since Q_{A^+} is positive for $Mg^+(3p\pi)$, the additional interactions represented by eqs 9 and 10 *both* contribute to the attractive forces for the $Mg^+(3p\pi)\cdot Rg$ states. (c) Finally, there is a negative quadrupole moment along the bond axis induced on the Rg atom by the electric field gradient from the positive charge *Z* (see third term in eq 5).

$$Q_{Rg} = \frac{-(Z)(\alpha_{Rg})}{R^3} \qquad (11)$$

This induced quadrupole moment Q_{Rg} interacts with the permanent quadrupole moment component Q_{A^+} of A^+ along the bond axis (ref 146, p 83, eq 2.185; see Appendix I). Allowing for the "self-energy" necessary to induce the quadrupole[164,165]

$$V(R) = \frac{+3(Q_{A^+})(Q_{Rg})}{R^5} \qquad (12)$$

Thus

$$V(R) = \frac{-3(Z)(\alpha_{RgQ})(Q_{A^+})}{R^8} \qquad (13)$$

and this term must be added to eq 5. When Q_{A^+} is positive (as for $Mg^+(3p\pi)$), this term (eq 13) also contributes favorably to the attractive forces.

2. Large Positive Polarizability of $Mg^+(3p\pi)$

The positive (perpendicular) dipole polarizability of the excited $Mg^+(3p\pi)$ state (polarizability tensor values of electronically excited states can be either positive or negative[1,65,145,146,176]) is also relatively large,[44] so that the calculated C_6 dispersion coefficient for $Mg^+(3p\pi)$ interacting with a Rg atom is not much less than that of the $Mg^+(3s)$ ion.

3. Minimal Axial Repulsion

Finally, the Rg atom approaches the Mg^+ excited-state ion along the nodal axis of the $Mg^+(3p\pi)$ orbital, so that repulsion is less than for the $Mg^+(3s)$ ground-state ion. This lack of repulsion allows all the attractive forces represented in eqs 5, 7, 9, 10, and 13 to extend to smaller *R*.

4. Z Values

Shown in Table 11 are the calculated *Z* values, both with and without the permanent quadrupole attractive terms (eqs 7, 9, 10, and 13) in the potential. It can be seen that with the inclusion of the two most important permanent quadrupole terms (eqs 7 and 9), the calculated *Z* values drop significantly. Addition of the two other quadrupole terms (eqs 10 and 13) further decreases *Z* to yield quite reasonable values. This indicates that a purely "physical" model can explain the very high bond energies of these $Mg^+(3p\pi)\cdot Rg$ excited states so that no *significant* "chemical" or charge-transfer interactions really need to be invoked to rationalize the very strong bonding. The same qualitative conclusion was also reached by Matsika and Pitzer[162] from ab initio calculations of the $Mg^+(3p\pi)\cdot Rg[^2\Pi]$ states (Rg = Ar, Xe).

On the other hand, the derived values of *Z* are a bit high for the experimentally based Rg = Ar and Kr data, so that our calculations cannot completely rule out a small amount of charge donation or Lewis acid/base "chemistry" beginning to appear for Rg atoms with lower ionization energies. [Note, however, there is *far more* than enough attractive energy to account for the D_e values in *all* the $Mg^+(3p\pi)\cdot Rg$ states even if we totally neglect the $1/R^7$ and $1/R^8$ terms! However, the *repulsive* energy in $M^+\cdot Rg$ complexes is always a substantial fraction (50 ± 15%) of the attractive energy, and our imposed model-potential requirement of rationalizing *all* of the R_e, D_e, *and* ω_e values is much more stringent than just qualitatively "accounting" for total attractive energy (at R_e) greater than D_e, as many authors do. It is wise to remember, in this regard, that bond strengths D_e are the $V(R)$ *minima* and are thus at the values of *R* (R_e) where the positive repulsion begins to rise more rapidly in absolute magnitude (per d*R* decrease) than does the negative attraction.] For example, the $Mg^+(^2P) + Xe(^1S_0)$ energy is only slightly lower than the $Mg(^1S_0) + Xe^+(^2P)$ energy. Unfortunately, there is no R_e value available for the $Mg^+(3p\pi)\cdot Xe$ state, even from ab initio calculations, but a rough estimate (by us) of $R_e = 2.55 \pm 0.15$ yields $Z = 1.19 \pm 0.30$. Then again (nothing is ever that simple, it seems), the lowest-energy "charge-transfer" $Mg(3s^2)\cdot Rg^+((5p\sigma)^2(5p\pi)^3)$ states of the same $^2\Pi$ symmetry

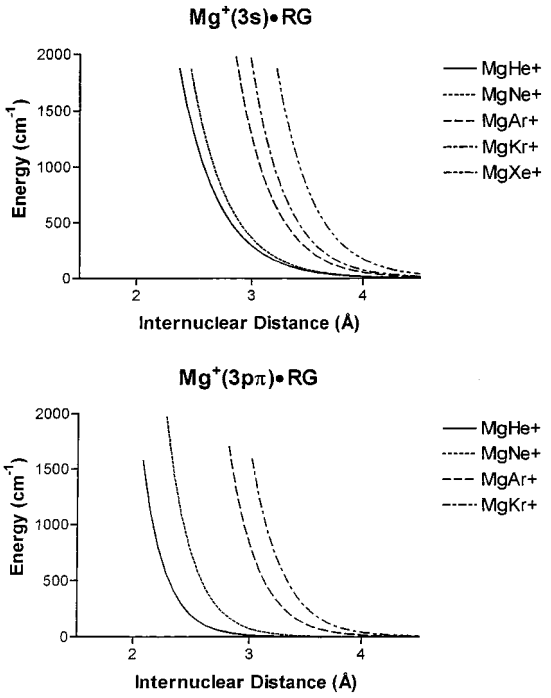

Figure 14. (Top) Plots of derived Ae^{-bR} curves for the $Mg^+(3s)$·Rg[$^2\Sigma^+$] ground states. (Bottom) Plots of derived Ae^{-bR} curves for the $Mg^+(3p\pi)$·Rg[$^2\Pi_{3/2}$] excited states.

must involve a "π-hole" on the Rg ion; there would thus be large, filled-shell $(3s\sigma)^2/(5p\sigma)^2$ repulsion (especially at the small R_e values for the $Mg^+(3p\pi)$·Rg states), and the quadrupole moment component along the bond axis would also contribute *repulsively*, as in the $Mg^+(3p\sigma)$·Rg states (see below). It is therefore an open question whether formal "charge-transfer" state mixing would truly be *stabilizing* for the wave functions of these high-energy $Mg^+(3p\pi)$·Rg[$^2\Pi$] states. (A competent, thoughtful, high-level ab initio study of all the relevant Mg^+Xe and $MgXe^+$ states would be quite interesting in this regard.)

5. Ae^{-bR} Repulsive Curves

It is important to examine the empirically derived Ae^{-bR} repulsive curves as well to see if they at least make qualitative sense. Shown in the bottom of Figure 14 are the repulsive curves for $Mg^+(3p\pi)$·Rg, for Rg = He, Ne, Ar, Kr. Since repulsion sets in at increasingly larger R as the "size" of the outer-shell electron cloud on the Rg atom increases, these curves do follow the expected qualitative trend.

For comparison, the Ae^{-bR} repulsive curves for the $Mg^+(3s)$·Rg ground states are shown in the top of Figure 14. The pattern of increasing repulsion with Rg "size" is also followed, as expected, but there are two important differences: (i) Consistent with the idea discussed above that repulsion in the $Mg(3p\pi)$·Rg states is minimized by the Rg atom approaching along the $Mg(3p\pi)$ nodal axis, the MgRg curves (for a given Rg) in the bottom of Figure 14 show *less* repulsion than those in the top of Figure 14. (ii) The relative *decrease* in repulsion from Rg = Ne to Rg = He is much *greater* for the $Mg^+(3p\pi)$·Rg states (bottom) than for the $Mg^+(3s)$·Rg states (top). This is consistent with our earlier postulate[156] that because the He atom does not have $p\pi$ electrons, there is no $p\pi/p\pi$ exchange repulsion. The (only slightly) smaller He atom can thus penetrate *much* closer to the $Mg^+(3p\pi)$ ion than can the Ne atom. Such an argument rationalizes nicely not only the unexpected observation that the $Mg^+(3p\pi)$·He state is more strongly bound than the $Mg^+(3p\pi)$·Ne state,[102,156] but also that the $Mg^+(3p\pi)$·He excited state (incredibly) is bound 35 times more strongly[156] than the $Mg^+(3s)$·He ground state (where $Mg^+(3s)$/He(1s) repulsion is large (see Table 4)). Similarly unexpected bonding trends are seen in the analogous, isoelectronic (but more weakly bound) Na(3s)·Rg and $Na(3p\pi)$·Rg neutral states (Rg = He, Ne) for the same reasons.[14]

6. Detailed Comparison of the $Mg^+(3p\pi)$·Ar Excited State and the $Mg^+(3s\sigma)$·Ar Ground State

In Table 12 we show the magnitudes of all the terms in eqs 5, 7, 9, 10, and 13 for the $Mg^+(3p\pi)$·Ar excited state and the $Mg^+(3s\sigma)$·Ar ground state. It can immediately be seen that the permanent quadrupole terms (eqs 7, 9, 10, and 13) play a large role in the strong bonding in the $Mg^+(3p\pi)$·Ar state (27% of the attraction at R_e) and that the dispersion terms (as for the $Mg^+(3s\sigma)$·Ar ground state) are also important, accounting for 30% of the attraction at R_e. The "charge/induction"-type terms in eq 5, then, account for a total of only 43% of the attractive forces

Table 12. Comparison of the Contributions of the Various Terms in Eqs 5, 7, 9, 10, and 13 for $Mg^+(3s)$·Ar versus $Mg^+(3p\pi)$·Ar at R_e for Each State

	$Mg^+(3s)$·Ar (Z = 0.99; R_e = 2.81 Å)		$Mg^+(3p\pi)$·Ar (Z = 1.19; R_e = 2.38 Å)	
terms	E (cm^{-1})	% total attraction	E (cm^{-1})	% total attraction
$1/R^4$ (ion/induced-dipole)	−1500	41	−4432	28
$1/R^6$ (ion/induced-quadrupole)	−241	7	−992	6
$1/R^6$ (C_6)	−814	22	−1951	12
$1/R^7$	−125	3.5	−752	5
$1/R^8$ (ion/induced-octopole)	−90	3	−430	3
$1/R^8$ (γ)	−17	0.5	−142	1
$1/R^8$ (C_8)	−829	23	−2881	18
$1/R^6$ (eq 7)			−1528	10
$1/R^6$ (eq 9)			−1528	10
$1/R^8$ (eq 10)			−527	3
$1/R^8$ (eq 13)			−681	4
total attraction	−3616	100	−15,844	100
Ae^{-bR} (repulsion)	+2326	64	+10,296	65
net	−1290	36	−5548	35

for the $Mg^+(3p\pi)$·Ar excited state versus 55% for the $Mg^+(3s\sigma)$·Ar ground state. It is also interesting to point out that our analysis indicates that the $1/R^4$ charge/induced-dipole force, assumed by most researchers to be dominant in all M^+/Rg interactions, *only accounts for 28% of the physical "bonding" in the* $Mg^+(3p\pi)$·*Ar state*. This is, in fact, probably the most important conclusion from our detailed, semiquantitative analysis of these strongly bound $Mg^+(3p\pi)$·Rg states.

B. $A^+(p\sigma)$·Rg States

No detailed spectroscopic information has ever been reported for the analogous $Mg^+(3p\sigma)$·Rg states, where the $Mg^+(3p)$ orbital is aligned *along* the bond axis, but an unresolved feature (apparently a continuum)[106] to the blue of the $Mg^+(3p) \leftarrow Mg^+(3s)$ atomic transitions can be assigned[106] to the transition from the moderately bound $Mg^+(3s)$·Ne($v'' = 0$) ground state to inner-wall repulsive portions of the $Mg^+(3p\sigma)$·Ne potential curve. This is consistent with ab initio calculations[162] which indicate that, in stark contrast to the $Mg^+(3p\pi)$·Rg[$^2\Pi$] states, the $Mg^+(3p\sigma)$·Rg[$^2\Sigma^+$] states are *much less* bound (in fact, hardly bound *at all*, at least for an M^+/Rg complex (calculated D_e values for Rg = Ar and Xe of 97 and 290 cm^{-1}, respectively[162])), and have much larger R_e values (calculated to be 5.2 and 4.8 Å, respectively[162]) than the $Mg^+(3s)$·Rg[$^2\Sigma^+$] ground states.

The weak bonds have been attributed[106,162] to the fact that for these states the p-orbital electron density is concentrated along the bond axis, so that the $Mg^+(3p\sigma)$/Rg σ-σ repulsion is greater (and sets in at larger R) than the analogous $Mg^+(3s)$/Rg σ-σ repulsion. This is certainly true (and is totally responsible for the very weak bonds and large R_e values of the isoelectronic $Na(3p\sigma)$·Rg[$^2\Sigma^+$] neutral states compared even to the very weakly bound Na(3s)·Rg[$^2\Sigma^+$] ground states[106,167]). For $Mg^+(np\sigma)$·Rg ions, however, the σ-alignment of the $Mg^+(np)$ quadrupole moment Q_{zz} also contributes *repulsively* (and substantially) to the Mg^+/Rg interaction. The $V(R)$ quadrupole terms in eqs 7, 9, and 13 are now all *positive* (and twice as large in magnitude, since the Q_{M^+} value for $Mg^+(3p\sigma)$ alignment is twice as large as and opposite in sign to the Q_{M^+} value for $Mg^+(3p\pi)$ alignment (see Appendix I)).

This unfavorable effect contributes significantly and partially accounts for the fact that the $Mg^+(3p\sigma)$·Rg bonds (Rg = Ar, Xe) are extremely weak (the strong ion/induced-dipole attractive term normally ensures at least reasonable bond strengths[3] for M^+ complexes of Ar and Xe). For the $Mg^+(3p\sigma)$·Ar state, at $R_e = 5.2$ Å (for $Z = 1.0$), the total repulsive contribution from the three quadrupole terms (eqs 4, 6, and 10) is +48 cm^{-1} while the total attraction, from the terms in eqs 2 and 7, is −168 cm^{-1} (most of which is from the long-range $1/R^4$ term: −131 cm^{-1}). For the ab initio D_e value of 97 cm^{-1}, this means that the Ae^{-bR} repulsive term need contribute only +23 cm^{-1} at $R_e = 5.2$ Å.

Table 13. Values of *A*, *b*, and *Z* Calculated for Transition-Metal-Ion States with Permanent Quadrupole Moments Using Eq 5 Only Compared to the Values Calculated with the Attractive Terms in Eqs 7, 9, 10, and 13 Added (same values of D_e, R_e, ω_e, etc., as in Tables 4−6)

M^+Rg state	Q_M+ (e − Å^2)[a]	A (cm^{-1})	b (Å^{-1})	Z
$V^+(3d^34s)$·Ar	(0)	2.68×10^7	3.240	1.01 ± 0.06
	+0.26[d][+0.27][c]	2.66×10^7	3.222	0.97 ± 0.06
$Co^+(3d^74s)$·Ar	(0)	4.04×10^7	3.485	0.96 ± 0.06
	+0.050[c]	4.02×10^7	3.480	0.95 ± 0.06
$Co^+(3d^8)$·Ar	(0)	1.57×10^8	4.252	1.02 ± 0.10
	0[b]	1.57×10^8	4.252	1.02 ± 0.10
$Hg^+(5d^96s)$·Ar	(0)	1.96×10^8	3.907	1.02 ± 0.07
	+0.18[c]	1.88×10^8	3.884	0.99 ± 0.07

[a] Q_M+ values were calculated using eqs B and C in Appendix I, with R^2_{nd} values taken from ref 158 or 159. The $nd\sigma$, $nd\pi$, $nd\delta$ occupations for each state are those shown in Tables 2 and 3. [b] $Q_M+ = 0$ for the $(3d\sigma)(3d\pi)^4(3d\delta)^3$ occupation of the $Co^+(3d^8\ ^3F)$·Ar[$^3\Delta_3$] ground state. [c] Reference 158. [d] Reference 159.

C. A^+·Rg States Where A^+ Is an Open-d-Shell Transition-Metal Ion

Many states of transition-metal ions A^+ have open d-shell configurations, so that their A^+/Rg electronic states can have permanent quadrupole moment components along the A^+/Rg bond axis (see Appendix I) which depend on the $d\sigma$, $d\pi$, and $d\delta$ alignment of all the outer-shell $A^+(nd)$ electrons in the particular A^+/Rg electronic state of interest. However, the nd orbitals for such states are much smaller than the 3p orbital in excited $Mg^+(3p)$, and at least for the well-characterized (and typical) states of transition-metal ions listed in Table 13, the net permanent quadrupole moment components Q_{A^+} along the bond axis are also quite small (but still positive or zero; the most stable electronic states observed tend to *minimize* $d\sigma$ occupation, usually leading to positive net quadrupole moment tensor components along the z-axis, analogous to the $Mg^+(3p\pi)$ case).

Shown in Table 13 are the effects on Z, A, and b of adding the attractive terms in eqs 7, 9, 10, and 13 to eq 5 for transition-metal-ion/Rg complexes. As can be seen, the derived repulsive curves are not greatly affected. The Z values do decrease by a few percent but are still quite consistent with the expected value of $Z = 1.00$, within the uncertainties. For the transition-metal ions A^+·Rg, then, the permanent quadrupole terms, although not entirely negligible, appear to be relatively unimportant, whereas for the $Mg^+(3p\pi)$·Rg cases, these quadrupole terms are essential in explaining the very strong bonding. (The R_e values for the transition metal A^+·Ar states with quadrupole moments in Table 13 are also larger than the $R_e = 2.38$ Å for the $Mg^+(2p\pi)$·Ar state, thus diminishing the relative importance of the $1/R^6$, $1/R^8$ permanent quadrupole terms; this may not always be true, however, especially for some $M^+(nd^n)$/Rg electronic states with smaller R_e values.)

VI. States in Which M^+He Is More Strongly Bound than M^+Ne

In general, the D_e values for particular M^+Rg states shown in Tables 2 and 3 increase with the Rg

polarizability, as generally expected. The only exceptions (for reliable ab initio calculations) are for a few M^+He versus M^+Ne states. There are two main categories of such states.

A. Excited $M^+(p\pi)$·Rg States

As discussed above, we believe that the larger D_e values for Rg = He versus Rg = Ne for such excited states as $Mg^+(3p\pi)$·Rg and $Be^+(3p\pi)$·Rg [see Table 3] are due to the lack of $p\pi$ electrons on the He atom, so that there is no $p\pi/p\pi$ exchange repulsion. The He atom can thus approach a $M^+(np\pi)$ state quite closely, so that the attractive $1/R^n$ forces are much greater at R_e than for Rg = Ne, even though the polarizability of He is a factor of 2 smaller than that of Ne. In a theoretical study, this was shown to be true for the analogous neutral $Na(3p\pi)$·Rg states.[14]

B. $M^+(nd^n)$·Rg States

Again, reliable ab initio calculations (by Bauschlicher et al.) indicate that some $M^+(3d^n)$·He states are more strongly bound than their $M^+(3d^n)$·Ne counterparts (see Tables 2 and 3). For some of these $M^+(3d^n)$·Rg states, there are $d\pi$ but no $d\sigma$ electrons, so that the lack of $p\pi$ electrons on He, as explained above, could explain the higher D_e values for the $M^+(3d^n)$·He states. Ground-state $V^+(3d^4)$·Rg[$^5\Sigma^+$], with $(d\pi)^2(d\delta)^2$ character, and excited-state $Ti^+(3d^3)$·Rg[$^4\Delta$], with $(d\pi)^2(d\delta)^1$ character, fall in this category.

However, there are other such cases in which there must be $d\sigma$ electrons present. For example, the filled-shell $Cu^+(d^{10})$·Rg[$^1\Sigma_g^+$] state must have two $d\sigma$ electrons, and any $Ni^+(3d^9)$·Rg states must have at least one $3d\sigma$ electron. Yet in both cases, the M^+He ion is more strongly bound than the M^+Ne ion. It appears that all such cases (for $d\sigma$ occupation) involve Co^+, Ni^+, and Cu^+, which are the smallest $3d^n$ ions (to the right in the 3d transition-element row). Thus, it is possible that because at smaller internuclear distances both $d\sigma/p\sigma$ and $d\pi/p\pi$ repulsion are important for Ne but only $d\sigma/p\sigma$ repulsion for He, the He atom has a slight advantage. [Note that the polarizabilities of Ne and He only differ by a factor of 2, so that only a small relative decrease in R due to decreased relative repulsion, given the $1/R^4$ dependence of the attractive forces, can tip the balance in favor of He.] This is not true for the larger M^+ ions further to the left: for states of Ti^+ and Cr^+ which formally have $d\sigma$ occupancy, for example, M^+Ne is bound more strongly than M^+He. There is also the possibility that subtle differences in $sd\sigma$ hybridization may be involved as well, as suggested by Bauschlicher, Langhoff, and Partridge.[180]

VII. Neglect of "Cutoff" Functions

Perhaps the greatest shortcoming of our approximate model-potential approach is that we make no attempt to account for the "cutoff" of long-range attractive terms which must occur as the electron clouds of the M^+ ion and the Rg atom interpenetrate. Although there are "cutoff" formulas which have been constructed[1,7,145,146] to account for such interpenetration, we have chosen not to include them in our model potentials. One main reason is simplicity. Our purpose here has been to compare the potential curves of a large variety of different kinds of A^+·Rg species near their R_e values in order to understand differences in the van der Waals bonding and not to reproduce only the very few A^+·Rg potential curves known accurately from very large to very small internuclear distances. Furthermore, although the percent error in the Ae^{-bR} repulsive curves derived from our model-potential analyses will not be negligible at R_e (after all, that is where *repulsion* due to electron-cloud interpenetration begins to rise faster than attraction as R decreases), we believe that the derived Ae^{-bR} curves will be mostly affected *similarly* by neglect of the "cutoff" phenomenon. The result is that our Ae^{-bR} curves will be very slightly *more* repulsive than analogous derived Ae^{-bR} repulsive curves with the inclusion of cutoff functions. This shift should be roughly the same for most A^+/Rg states, however. Thus, our *comparison* of derived Ae^{-bR} curves should still be qualitatively (even semi-quantitatively) valid but will not reproduce the high-energy, repulsive portions of reliable ab initio A^+·Rg potential curves.

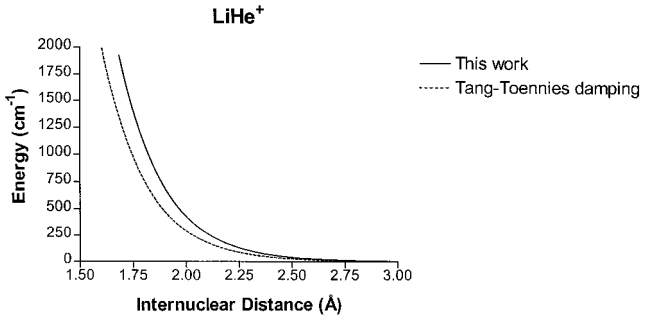

Figure 15. (—) Plot of our derived Ae^{-bR} repulsive curve for Li^+He. (- - -) Plot of Ae^{-bR} repulsive curve derived by Wright and co-workers[177] using a very similar model potential but with Tang−Toennies damping functions and fixing the charge on the Li^+ ion at +1.00.

In effect, any "damping" is empirically included in the exponential Ae^{-bR} Buckingham "repulsive" term in our model potential. Shown in Figure 15 is a comparison of our derived repulsive curve for Li^+He ($A = 5.57 \times 10^6$ cm^{-1}; $b = 4.734$ Å^{-1}) to a repulsive curve for Li^+He ($A = 4.58 \times 10^6$ cm^{-1}; $b = 4.828$ Å^{-1}) derived recently with similar attractive terms but with Tang−Toennies cutoff functions included in those attractive terms.[177] As can be seen, the two curves are very similar and differ by about 30% at any given value of R.

A second reason for not including some sort of cutoff functions are our doubts that they are really *quantitatively* valid. For quadrupole attractive terms, for example, appropriate cutoff functions have not yet been discussed generally, especially for different quadrupole alignments along the bond axis.

VIII. Spin–Orbit Coupling in M^+Rg States

A. Effects of Spin–Orbit Coupling on Bonding in M^+Rg States

For open-shell p, d, etc., states of an M^+ ion, there is coupling between spin (S) and orbital (L) angular momentum in the free M^+ ion, resulting in J levels of different energies. This "spin−orbit coupling" occurs because[161] the electron(s) spend(s) some time very near the positively charged nucleus, where its velocity is very high. The high magnetic field generated by this "orbital" motion (current) can interact strongly with the "spin" magnetic moment of the electron. (From the point of view of the electron, it experiences a magnetic field due to the positive nucleus circling around *it*!) The coupling due to this "current" increases rapidly with nuclear charge, so "heavy" atoms have much larger spin−orbit coupling constants A_{LS} (proportional to the total splitting of the J-levels for a given configuration) than do "light" atoms.

When such M^+ states interact with a Rg atom to form M^+Rg states, there is a recoupling[161,167,171] of orbital and spin angular momentum along the bond axis, since the only truly "good" quantum number is now Ω, the projection of the total electronic angular momentum *along* this axis. For the usual Hund's case a, where the molecular spin−orbit coupling constant $A_{\Lambda\Sigma}$ is smaller than the molecular potential energy $|V(R)|$ [$|A_{\Lambda\Sigma}| \ll D_e$, near the bond length R_e], the bond-axis projections of the total orbital angular momentum, Λ, and total spin angular momentum Σ, are also meaningful quantum numbers and couple to form states characterized by the values of Ω allowed for given Λ, Σ values.

For pure Hund's case a, the effect of spin−orbit coupling on bonding is negligible, since the D_e value is much greater than the small energy splittings of the Ω levels. However, when the $|A_{\Lambda\Sigma}|$ constant starts to become a significant fraction of D_e, one begins to see the approach to Hund's case c, where in the limit Λ and Σ are no longer good quantum numbers and *only* Ω survives.

This approach to case c can be treated quantitatively by constructing the appropriate spin−orbit interaction matrixes to describe each Λ, Σ, and Ω state. This is treated in detail elsewhere.[167] The net result, however, is that the wave functions of case a states with different Λ, Σ values but the same value of Ω begin to "mix" due to the spin−orbit part of the Hamiltonian. In the simplest case, the interactions of $M^+(np\ ^2P_{1/2,3/2})$ spin−orbit states with a Rg atom, for pure case a there are three electronic states of the $M^+(np)Rg$ molecule possible: $^2\Pi_{3/2}$, $^2\Pi_{1/2}$, and $^2\Sigma^+_{1/2}$. For pure case a conditions, both $^2\Pi_\Omega$ states correspond (essentially) to pure $M^+(p\pi)\cdot Rg$ alignment and are similar in energy at R_e, being split only by the (relatively) small value of $A_{\Lambda\Sigma}$. For such conditions, the $M^+(^2P_{1/2,3/2})$ asymptotic splitting would be 3/2 of the $M^+(np\pi)\cdot Rg[^2\Pi_{1/2,3/2}]$ molecular splitting if there is no effect on the M^+ spin−orbit coupling by the bonding of the Rg atom (but see below). Thus, $D_e(^2\Pi_{1/2})$ will be less than $D_e(^2\Pi_{3/2})$ by only $^1/_2A_{\Lambda\Sigma}$, a negligible amount for pure case a conditions. The $^2\Pi_{1/2,3/2}$ states are then "pure" $M^+(p\pi)$ in character, and the $^2\Sigma^+$ state is "pure" $M^+(p\sigma)$ in character.

However, even when case a is still a reasonably good description of the angular-momentum coupling, as $A_{\Lambda\Sigma}$ becomes a substantial fraction of $D_e(^2\Pi)$ the D_e values of the $^2\Pi_{3/2}$ and $^2\Pi_{1/2}$ multiplets can become quite different, percent-wise (D_e values with respect to the $M^+(^2P_{3/2})$ and $M^+(^2P_{1/2})$ atomic states to which these states dissociate adiabatically, respectively, at $R = \infty$). For example (see below), the bond energies of the $^2\Pi_{1/2}$ and $^2\Pi_{3/2}$ multiplets of $Ba^+(6p\pi)\cdot Ar[^2\Pi]$ are estimated (see Table 3) to be ~1600 and ~2100 cm^{-1}, respectively.

As $A_{\Lambda\Sigma}$ increases relative to D_e in these kinds of states, the two case a $^2\Sigma_{1/2}{}^+$ and $^2\Pi_{1/2}$ states with the same $\Omega = {}^1/_2$ begin to "mix" and each no longer has pure $M^+(p\sigma)$ and pure $M^+(p\pi)$ character, respectively. In fact, at the case c limit, where $A_{\Lambda\Sigma} \gg D_e(^2\Pi)$, both $\Omega = {}^1/_2$ states will have *completely* mixed (but different) $M^+(p\sigma,p\pi)$ character and can no longer really be described in terms of p-orbital "alignment" at all. On the other hand, the $^2\Pi_{3/2}$ state is the *only* case "a" $\Omega = 3/2$ state and remains "pure" $M^+(p\pi)$ in character all the way from pure case "a" to pure case "c" (and at all moderate internuclear distances R for a given state). [Because of this, the $^2\Pi_{3/2}$ multiplet component of $M^+(np\pi)[^2\Pi_\Omega]$ states is the appropriate state for our model-potential analyses (see above), which do not include spin−orbit coupling.] Similarly, for $M^+(nsnp\ ^3\Pi,^1\Pi)\cdot Rg$ states, only the $^3\Pi_2$ multiplet remains "pure-π" in character for all values of $A_{\Lambda\Sigma}$, while the $^1\Sigma_0^+ + {}^3\Pi_0{}^+$, $^1\Pi_1/{}^3\Pi_1/{}^3\Sigma_1^+$, and $^3\Sigma_0^- - {}^3\Pi_0-$ groups of states are "mixed" to various degrees by spin−orbit coupling.

Spin−orbit coupling in $A^+\cdot Rg$ states where A^+ is an open-shell "*n*d" state can be quite complex, and such cases are not discussed here.

B. Increase in Magnitudes of $M^+\cdot Rg$ Molecular Spin–Orbit Coupling Constants by Mixing of Rg Character into Predominantly M^+ Wave Functions: The "Heavy-Atom" Effect

It has been observed, in several open-shell π states of M^+Rg (and MRg) van der Waals complexes,[23,25,26,29,71,167] that the measured molecular spin−orbit coupling constants $A_{\Lambda\Sigma}$ are often greater than those calculated only on the basis of the atomic A_{LS} constants of the open-shell p-orbital state of M^+ (assuming Hund's case a recoupling of spin and orbital angular momenta along the bond axis). The molecular spin−orbit constants also increase in the Ne < Ar < Kr < Xe "heavy-atom" order and for a given state; the molecular spin−orbit constant increases as the vibrational quantum number v decreases, maximizing at $v = 0$.

This effect is now known[162] to be caused by direct, repulsive exchange overlap of $p\pi$ orbitals on M^+ and $p\pi$ orbitals on the Rg atom, which increases dramatically as $\langle R\rangle_v$ decreases when v decreases (due to anharmonicity). In molecular orbital terms, it is due to formation of π^* antibonding orbitals by mixing of small amounts of $Rg(p\pi)$ orbital character into the dominant $M^+(p\pi)$ orbital character. In terms of our model potential, it increases rapidly as the Ae^{-bR}

Table 14. Molecular Spin−Orbit Constants $A_{\Lambda\Sigma}$ for Various States

state	$A_{\Lambda\Sigma}$ (cm^{-1}) expected[a]	observed
$Mg^+(3p\pi)$·Ne[$^2\Pi$]	61.0	∼64[106]
$Mg^+(3p\pi)$·Ar[$^2\Pi$]	61.0	76[29]
$Mg^+(3p\pi)$·Kr[$^2\Pi$]	61.0	144[29]
$Mg^+(3p\pi)$·Xe[$^2\Pi$]	61.0	268[29]
$Na(3p\pi)$·Ar[$^2\Pi$]	11.5	∼20[167,b]
$Na(3p\pi)$·Kr[$^2\Pi$]	11.5	48.7[174,b]
$Na(3p\pi)$·Xe[$^2\Pi$]	11.5	112.2[175,b]
$Be^+(2p\pi)$·Ar[$^2\Pi$]	4.4	43[71]
$Be^+(2p\pi)$·Kr[$^2\Pi$]	4.4	166[25]
$Be^+(2p\pi)$·Xe[$^2\Pi$]	4.4	∼360[26]
$Li(2p\pi)$·Ne[$^2\Pi$]	0.23	2.77[172]
$Li(2p\pi)$·Ar[$^2\Pi$]	0.23	15.8[173,b]

[a] $A_{\Lambda\Sigma} = {}^2/_3 A_{LS}$, where A_{LS} is the atomic spin−orbit coupling constant for the state of the atom or atomic ion of interest. [b] Our extrapolated estimate.

term increases in magnitude when $\langle R \rangle_v$ becomes smaller. For light M^+ ions such as $Mg^+(3p\ ^2P_J)$, where the SO coupling constant is small, mixing of only tiny amounts of Rg(npπ) character, where the SO coupling constants are large (especially for Kr and Xe), can *dramatically* increase the molecular SO coupling constant $A_{\Lambda\Sigma}$ compared to that expected from the light M^+ ions only. For example, the A_{LS} constant for $Mg^+(3p)$ is only 91 cm^{-1}, compared to values of 782, 1649, 5220, and 9129 cm^{-1} for Ne(2p), Ar(3p), Kr(4p), and Xe(5p), respectively.[29,106]

Without mixing of Rg(npπ) character, the $^2\Pi_{1/2}/^2\Pi_{3/2}$ splitting in $Mg^+(3p\pi)$·Rg[$^2\Pi$] states is predicted to be 61.0 cm^{-1}, in the Hund's case a molecular limit.[29,39,161,167] The $^2\Pi_{1/2}/^2\Pi_{3/2}$ splittings of $Mg^+(3p\pi)$·Rg[$^2\Pi$] states ($v' = 0$) have been *measured*[29] to be ∼64, 76, 144, and 268 cm^{-1} for Rg = Ne, Ar, Kr, and Xe, respectively. These larger values can be explained by Ne(2pπ), Ar(3pπ), Kr(4pπ), and Xe(5pπ) mixing of only ∼0.6%, ∼1.5%, ∼2.4%, and ∼3.4%, respectively, which are really quite low values. The ab initio calculations of Pitzer[162] indicate ∼2% mixing of Ar(3pπ) character into the π^* molecular orbital at his calculated R_e value for $Mg^+(3p\pi)$·Ar[$^2\Pi$]. Qualitatively similar increases in the molecular spin−orbit constant have been observed for the isoelectronic, neutral $Na(3p\pi)$·Rg[$^2\Pi$] states as well as for the analogous $Be^+(2p\pi)$·Rg[$^2\Pi$] states (and the isoelectronic $Li(2p\pi)$·Rg[$^2\Pi$] states), see Table 14.

In contrast, for $M^+(np\pi)$·Rg states for which M is a heavy atom, any small mixing of Rg character has little effect (percent-wise) on the (already large) molecular SO constant $A_{\Lambda\Sigma}$ due to M^+ alone. For example, the $^2\Pi_{1/2}/^2\Pi_{3/2}$ splitting in $Ba^+(6p\pi)$·Ar[$^2\Pi$] was measured to be 1186 cm^{-1}, as compared to the value of 1127 cm^{-1} predicted based on A_{LS} of $Ba^+(6p\pi)$ (and Hund's case a coupling). (Also, since the measured $A_{\Omega\Sigma}$ *increases* from $v' = 0$ to $v' = 1$, even the slightly higher value than predicted is merely due to incomplete recoupling to case a conditions, since $A_{\Lambda\Sigma}$ is a *substantial* fraction of D_e'' for these states.)

IX. A Final Word

Our model-potential analysis has not been designed to reproduce complete potential energy curves $V(R)$ from R values much greater than R_e (where $V(R)$ approaches zero) to R values much smaller than R_e (where $|V(R)| \gg |D_e|$), but in fact was designed for the following. (i) To see if properly calculated dispersion and induction attractive terms as well as an empirical Ae^{-bR} repulsive term can reproduce R_e, D_e, and ω_e values with values of Z close to the formal charge on the atomic ion. This obviously biases our model "potential curves" toward reproducing the $V(R)$ potentials accurately near R_e but not *necessarily* at very large values of R (where Z for an A^+ ion must equal 1.00 exactly) or very small values of R (especially). (ii) To compare many different A^+·Rg electronic state potential curves in hopes of understanding the interesting variations in the attractive and repulsive terms which influence "bond-making", using the most widely available information (D_e, ω_e) about the different potential curves near R_e.

We think this has been a useful and interesting exercise, but we know it will not sit well at all with some purists, who would rather reproduce a few *complete* potential curves to a higher degree of accuracy. So be it. For the wide variety of A^+·Rg states we have been able to analyze successfully (and reasonably) with our model, in a qualitative manner, this would require either extremely sophisticated model potentials, including damping functions (see above), or super-high-level, "break-the-bank" ab initio calculations. We will leave such endeavors to other researchers in the future.

X. Acknowledgments

Support for this work has been provided by the National Science Foundation, the Petroleum Research Fund (administered by the American Chemical Society), and the University of Utah Research Foundation. W.H.B. acknowledges stimulating (as always) conversations with his colleagues Michael Morse, Jack Simons, and Peter Armentrout. Helpful correspondence with Jeremy Hutson, Maciej Gutowski, Jim Harrison, and especially Grzegorz Chalasinski, concerning permanent and induced multipole moments (and their interactions), is also gratefully acknowledged. We thank Jim Harrison for communicating his quadrupole moment calculations for some first-row transition-metal M^+ states before publication and Tim Wright for communicating the results of his ab initio calculations of M^+Rg states before publication. We acknowledge the use of the computer facilities provided by the Center for High Performance Computing at the University of Utah. (The SP has been partially funded by NSF Grant No. CDA 9601580 and a Shared University Research (SUR) grant from IBM.) We are also very grateful to C. Froese-Fischer for allowing us to use her numerical Hartree−Fock program. Finally, we thank Ryan R. Julian, Allen W.-K. Leung, and especially Katherine L. Burns for their earlier contributions to the development of our model-potential analysis approach.

XI. Appendix I

A. Quadrupole Moments of States of Atomic Ions or Neutral Atoms

We adopt the following definition for the quadrupole moment tensor component of an atomic ion (or neutral atom) along a particular direction (the Z axis)[1,145,146]

$$Q_{zz} = -\,{}^1/_2(\mathrm{e})\sum_{i=1}^{n}\langle 3Z^2 - R^2\rangle_i \qquad \text{(A)}$$

where e is the unit charge, and where the sum is over all p, d, f, etc., electrons which are not in filled shells. Note that some authors omit the factor "$^1/_2$", which is unfortunate since it can cause a lot of confusion. Our definition is consistent with that used (mostly) in describing quadrupole moments of molecules.[146] The Z-axis is usually chosen to be the "unique" axis of the atomic state, so that $Q_{zz} = -^1/_2\, Q_{xx} = -^1/_2\, Q_{yy}$ (the quadrupole charge distribution is formally described as a traceless second-rank tensor). The sign of Q_{zz} is defined to be *negative* for a $-/++/-$ linear quadrupole (like CO_2, or Al($3s^2$ 3p), directed along the Z axis). Thus, Q_{zz} is usually the value referred to as "the" quadrupole moment in the literature. Again, one must be careful, however, since some authors define the "quadrupole moment" of an atom as that tensor component for the axis along which the J and M_J values are maximum. For example, the first experimental measurement of a quadrupole moment of an atom,[182] Al($3s^2 3p\ ^2P_{3/2}$), was quoted to be $+2.53 \pm 0.15$ au, which is for the Al(3p) orbital aligned in a pπ fashion ($p_{\pm 1}$) with respect to the external space-fixed axis in the experiment. For our convention, then, Q_{zz} (Al($3s^2 3p\ ^2P_{3/2}$)) $= -5.06 \pm 0.30$ au (pσ(p_o) alignment). Their quoted value corresponds to $Q_{xx}(=Q_{yy})$ in our convention.

The atomic quadrupole moment definition can be separated into radial and angular parts,[159,183] since $Z = R\cos\theta$

$$Q_{zz} = -\,{}^1/_2\,(e)\sum_{i=1}^{n}\langle 3\cos^2\theta - 1\rangle_i\cdot\langle R^2\rangle_i \qquad \text{(B)}$$

where $\langle R^2\rangle$ is the expectation value of R^2 for each p, d, f, etc., orbital i, and[184]

$$\langle 3\cos^2\theta - 1\rangle = -\left(\frac{3m_l^2 - l(l+1)}{l(2l-1)}\right)\cdot\left(\frac{2l}{2l+3}\right) \qquad \text{(C)}$$

is the factor which describes the alignment (m_l) of the electron i with angular momentum l along the Z-axis (pσ, pπ; dσ, dπ, dδ; etc.). Equations (B) and (C) are quite useful, since they allow us to estimate the "true" quadrupole moment tensor component along an axis Z (which we take to be the bond axis of an A^+/Rg molecule) if we know the alignment of all the outer-shell p, d orbitals in the molecular electronic state of interest (we thus abandon the "convention" that the Z-axis is the "unique" axis for the free atomic A^+ ion tensor, and pick our "direction" to be the bond-axis direction in the electronic state of A^+/Rg of interest), and if we can obtain estimates of $\langle R^2\rangle$, for each np, nd, etc., electron of interest for the state of interest.

In eqs 6−10, $''Q_{A^+}'' = Q_{zz}$ from eq B, with the Z axis being the A^+/Rg bond-axis. Thus, the Q_{A^+} contributions from single pσ, pπ, dσ, dπ, or dδ electrons are

$$Q_{A^+}(np\pi) = +\,{}^1/_5\langle R^2_{np}\rangle$$

$$Q_{A^+}(np\sigma) = -\,{}^2/_5\langle R^2_{np}\rangle$$

$$Q_{A^+}(nd\delta) = +\,{}^2/_7\langle R^2_{nd}\rangle$$

$$Q_{A^+}(nd\pi) = -\,{}^1/_7\langle R^2_{nd}\rangle$$

$$Q_{A^+}(nd\sigma) = -\,{}^2/_7\langle R^2_{nd}\rangle$$

XII. References

(1) Stone, A. J. *The Theory of Intermolecular Forces*; Clarendon Press: Oxford, 1996.
(2) *Chem. and Eng. News* **2000**, *78* (19), 15.
(3) Mo, Y.; Gao, J.; Peyerimhoff, S. D. *J. Chem. Phys.* **2000**, *112*, 5530.
(4) Koutselos, A. D.; Mason, E. A.; Viehland, L. A. *J. Chem. Phys.* **1990**, *93*, 7125.
(5) Røeggen, I.; Skullerud, H. R. *J. Phys. B* **1992**, *25*, 1795.
(6) Viehland, L. A. *Chem. Phys.* **1983**, *78*, 279.
(7) Ahlrich, R.; Böhm, H. J.; Brode, S.; Tang, K. T.; Toennies, J. P. *J. Chem. Phys.* **1988**, *88*, 6290 and references therein.
(8) Ahmadi, G. R.; Røeggen, I. *J. Phys. B* **1994**, *27*, 5603.
(9) Park, S. J.; Lee, Y. S.; Jeung, G.-H. *Chem. Phys. Lett.* **1997**, *277*, 208.
(10) Olson, R. E.; Liu, B. *Chem. Phys. Lett.* **1979**, *62*, 242.
(11) Bauschlicher, C. W., Jr.; Partridge, H.; Langhoff, S. R. *Chem. Phys. Lett.* **1990**, *165*, 272.
(12) Gatland, I. R. *J. Chem. Phys.* **1981**, *75*, 4162.
(13) Bauschlicher, C. W., Jr.; Partridge, H.; Langhoff, S. R. *J. Chem. Phys.* **1989**, *91*, 4733.
(14) Bililign, S.; Gutowski, M.; Simons, J.; Breckenridge, W. H. *J. Chem. Phys.* **1994**, *100*, 8212.
(15) Ahmadi, G. R.; Almlöf, J.; Røeggen, I. *Chem. Phys.* **1995**, *199*, 33.
(16) Senff, U. E.; Burton, P. G. *Mol. Phys.* **1986**, *58*, 637.
(17) Partridge, H.; Bauschlicher, C. W., Jr.; Langhoff, S. R. *J. Phys. Chem.* **1992**, *96*, 5350.
(18) Nyeland, C.; Tang, K. T.; Toennies, J. P. *Chem. Phys.* **1990**, *147*, 229.
(19) Mosszynski, R.; Wormer, P. E. S.; Viehland, L. A. *J. Phys. B* **1994**, *27*, 4933.
(20) Freitag, A.; Van Wüllen, Ch.; Staemmler, V. *Chem. Phys.* **1995**, *192*, 267.
(21) Pyykko, P. *J. Am. Chem. Soc.* **1995**, *117*, 2067.
(22) Schröder, D.; Schwarz, H.; Hrusak, J.; Pyykko, P. *Inorg. Chem.* **1998**, *37*, 624.
(23) Subbaram, K. V.; Coxon, J. A.; Jones, W. E. *Can. J. Phys.* **1976**, *54*, 1535.
(24) Goble, J. H.; Hartman, D. C.; Winn, J. S. *J. Chem. Phys.* **1977**, *67*, 4206.
(25) Coxon, J. A.; Jones, W. E.; Subbaram, K. V. *Can. J. Phys.* **1977**, *55*, 254.
(26) Coxon, J. A.; Jones, W. E.; Subbaram, K. V. *Can J. Phys.* **1975**, *53*, 2325.
(27) Spurlock, C. T.; Pilgrim, J. S.; Duncan, M. A. *J. Chem. Phys.* **1995**, *103*, 3293. Spurlock, C. T.; Pilgrim, J. S.; Duncan, M. A. *J. Chem. Phys.* **1996**, *105*, 7876.
(28) Massick, S.; Breckenridge, W. H. *Chem. Phys. Lett.* **1996**, *257*, 465.
(29) Pilgrim, J. S.; Yeh, C. S.; Berry, K. R.; Duncan, M. A. *J. Chem. Phys.* **1994**, *100*, 7945.
(30) Kaup, J. G.; Breckenridge, W. H. *J. Chem. Phys.* **1997**, *107*, 2180.
(31) Bauschlicher, C. W., Jr.; Partridge, H. *Chem. Phys. Lett.* **1995**, *239*, 241.
(32) Kaup, J. G.; Breckenridge, W. H. *J. Chem. Phys.* **1997**, *107*, 4451.
(33) Pullins, S. H.; Scurlock, C. T.; Reddic, J. E.; Duncan, M. A. *J. Chem. Phys.* **1996**, *104*, 7518.
(34) Czuchaj, E.; Rebentrost, F.; Stoll, H.; Preuss, H. *Chem. Phys.* **1996**, *207*, 51

(35) Buthelezi, T.; Bellert, D.; Lewis, V.; Brucat, P. J. *Chem. Phys. Lett.* **1995,** *246*, 145. The value of D_e for the $Ca^+Kr(^2\Sigma^+)$ state obtained by these authors, 840 ± 100 cm^{-1}, is far too low and appears to be the result of an incorrect D_e' value obtained from only three bands to the upper state, $Ca^+(3d\ ^2D_J)$·$Kr(^2\Sigma^+)$, one of them quite weak, see ref 85. We also quote the Birge−Sponer D_e' value for $Ca^+Ar(^2\Sigma^+)$ since the LeRoy−Bernstein method also used by the authors to estimate D_e' is not valid far from the upper-state dissociation limits.
(36) Lüder, C.; Prekas, D.; Vourliotaki, A.; Velegrakis, M. *Chem. Phys. Lett.* **1997**, *267*, 149.
(37) Lüder, C.; Velegrakis, M. *J. Chem. Phys.* **1996**, *105*, 2167.
(38) Prekas, D.; Feng, B.-H.; Velegrakis, M. *J. Chem. Phys.* **1998**, *108*, 2712.
(39) Panov, S. I.; Williamson, J. M.; Miller, T. A. *J. Chem. Phys.* **1995**, *102*, 7359.
(40) Bridge, N. J. *J. Mol. Spectrosc.* **1972**, *42*, 370.
(41) Linn, S. H.; Brom, J. M., Jr.; Tzeng, W.-B.; Ng, C. Y. *J. Chem. Phys.* **1985**, *82*, 648.
(42) Liao, C. L.; Ng, C. Y. *J. Chem. Phys.* **1986**, *84*, 1142.
(43) Martrenchard-Barra, C.; Jouvet, C.; Dedonder-Lardeux, C.; Solgadi, D. *J. Chem. Phys.* **1993**, *98*, 5281.
(44) Leung, A. W. K.; Breckenridge, W. H. Unpublished ab initio calculations. (Basis set same as ref 156; CISD(T) level of correlation.)
(45) Onda, K.; Tasaka, T.; Hishikawa, A.; Yamanouchi, K. In *Structures and Dynamics of Clusters*; Universal Academic Press: New York, 1996; pp 347−355.
(46) Onda, K.; Yamanouchi, K. *J. Chem. Phys.* **1995**, *102*, 1129.
(47) Onda, K.; Yamanouchi, K.; Okunishi, M.; Tsuchiya, S. *J. Chem. Phys.* **1994**, *101*, 7290.
(48) Estimated from parameters for the first triplet Rydberg state of ZnAr, see ref 49 and text.
(49) Bennett, R. R.; Breckenridge, W. H. *J. Chem. Phys.* **1990**, *92*, 1588.
(50) Estimated from parameters for the first triplet Rydberg state of CdAr, see refs 51 and 52 and text.
(51) Bennett, R. R.; Breckenridge, W. H. *J. Chem. Phys.* **1992**, *96*, 882.
(52) Czajkowski, M.; Bobkowski, R.; Krause, L. *Phys. Rev. A* **1992**, *45*, 6451.
(53) Heidecke, S. A.; Fu, Z.; Colt, J. R.; Morse, M. D. *J. Chem. Phys.* **1992**, *97*, 1692.
(54) From extrapolations of Al·Rg Rydberg state values to $n = 4$, see ref 53.
(55) From estimates based on the R_e values of the Al(4s)·Rg Rydberg states, see refs 56 and 57.
(56) McQuaid, M. J.; Gole, J. L.; Heaven, M. C. *J. Chem. Phys.* **1990**, *92*, 2733.
(57) Fu, Z.; Massick, S.; Kaup, J. G.; Benoist d'Azy, O.; Breckenridge, W. H. *J. Chem. Phys.* **1992**, *97*, 1683.
(58) Alexander M.; Dagdigian, P. Private communication.
(59) Polak-Dingels, P.; Rajan, M. S.; Gislason, E. A. *J. Chem. Phys.* **1982**, *77*, 3983.
(60) Park, S. J.; Kim, M. C.; Lee, Y. S.; Jeung, G.-H. *J. Chem. Phys.* **1997**, *107*, 2481.
(61) Calculated by us by fitting several ab initio points of the potential curve nearest the minimum, R_e, to a Morse function. (Isotope-abundance-weighted atomic masses were used.)
(62) Estimated from the R_e values for higher-energy triplet excited states of the CaRg van der Waals molecules, see refs 63 and 91.
(63) Kaup, J. G.; Breckenridge, W. H. *J. Chem. Phys.* **1997**, *107*, 5283.
(64) Read, J. P.; Buckingham, A. D. *J. Am. Chem. Soc.* **1997,** *119*, 9010 and references therein.
(65) Hirschfelder, J. O.; Curtiss, C. F.; Bird, R. B. *Molecular Theory of Gases and Liquids*; Wiley: New York, 1954.
(66) Estimated from R_e values of the first triplet Rydberg state of the MgRg van der Waals molecule, see ref 67.
(67) Kaup, J. G.; Leung, A. W. K.; Breckenridge, W. H. *J. Chem. Phys.* **1997**, *107*, 10492.
(68) Values lowered by ∼80 cm^{-1} from those quoted in refs 41 and 42 to correct for apparent field-ionization lowering of the ionization energy (correction was determined from effective IP of Hg atom shown in Figure 1a of ref 42).
(69) Røeggen, I.; Skullerud, H. R.; Elford, T. *J. Phys. B.* **1996**, *29*, 1913.
(70) Moszynski, R.; Jeziorski, B.; Dierckson, G. H. F.; Viehland, L. A. *J. Chem. Phys.* **1994**, *101*, 4697.
(71) Tai, G.; Verma, R. D. *J. Mol. Spectrosc.* **1995,** *173*, 296.
(72) $D_e = \omega_e^2/4\omega_e x_e$ (linear Birge−Sponer plot).
(73) Calculated from the recommended D_e'' and ω_e'' values for the ground state listed in Table 2, the recommended ω_e' values for the upper-state listed in Table 3, $v_{o,o}$ values, and a thermochemical cycle: $D_o' = D_o'' - v_{o,o} + E_{atomic}$, where E_{atomic} is the difference in energy of the asymptotic atomic states: $D_e = D_o + {}^1/_2\omega_e$.
(74) LeRoy, R. J. *J. Chem. Phys.* **1994**, *101*, 10, 217.
(75) Fanourgakis, G. S.; Farantos, S. C. *J. Phys. Chem.* **1996**, *100*, 3900.
(76) Gatland, I. R.; Morrison, W. F.; Ellis, H. W.; Thackston, M. G.; McDaniel, E. W.; Alexander, M. H.; Viehland, L. A.; Mason, E. A. *J. Chem. Phys.* **1977**, *66*, 5121.
(77) Dunning, T. H., Jr.; Valley, M.; Taylor, H. S. *J. Chem. Phys.* **1978**, *69*, 2672.
(78) Simpson, R. W.; Harland, P. W.; MacClagan, R. G. A. R.; Smith, D.; Adams, N. G. *Int. J. Mass Spectrom. Ion Processes* **1989**, *90*, 193.
(79) Jennis, E. D.; Wong, M. W.; Burgi, H.-B.; Radom, L. *J. Mol. Struct.* **1992**, *261*, 385.
(80) Hillier, I. H.; Guest, M. F.; Ding, A.; Karlan, J.; Weise, J. *J. Chem. Phys.* **1979**, *70*, 864.
(81) Xantheas, S. S.; Fanourgakis, G. S.; Farantos, S. C.; Velegrakis, M. *J. Chem. Phys.* **1998**, *108*, 46.
(82) Hammond, B. L.; Lester, W. A., Jr.; Braga, M.; Taft, C. A. *Phys. Rev. B* **1990**, *41*, 10447.
(83) Liebman, J. F.; Allen, L. C. *J. Am. Chem. Soc.* **1970**, *92*, 3539.
(84) Kirkpatrick, C. C.; Viehland, L. A. *Chem. Phys.* **1988**, *120*, 235.
(85) Heinemann, C.; Koch, W.; Partridge, H. *Chem. Phys. Lett.* **1998**, *286*, 131.
(86) Willey, K. F.; Yeh, C. S.; Duncan, M. A. *Chem. Phys. Lett.* **1993**, *211*, 156. (There are observations and interpretations in this MATI experiment which are unfortunately inconsistent with several other theoretical and experimental findings.)
(87) Partridge, H.; Bauschlicher, C. W., Jr. Private communication quoted in ref 86.
(88) Viehland, L. A.; Hampt, D. S. *J. Chem. Phys.* **1992**, *97*, 4964.
(89) LeRoy, R. J.; Lam, W. *Chem. Phys. Lett.* **1980**, *71*, 544.
(90) Monteiro, T. S.; Cooper, I. L.; Dickenson, A. S.; Lewis, E. L. *J. Phys. B* **1975**, *8*, 2708.
(91) Kaup, J. G.; Breckenridge, W. H. *J. Chem. Phys.* **1997**, *107*, 5676.
(92) Cooper, D. L.; Wilson, S. *Mol. Phys.* **1981**, *44*, 161.
(93) Wang, M. W.; Radom, L. *J. Phys. Chem.* **1989**, *93*, 6303.
(94) Augustin, S. D.; Miller, W. H.; Pearson, P. K.; Schaefer, H. F., III *J. Chem. Phys.* **1973**, *58*, 2845.
(95) Harrison, S. W.; Henderson, G. A.; Masson, L. J.; Solomon, P. *Astrophys. J.* **1974**, *189*, 605.
(96) Koch, W.; Liu, B.; Frenking, G. *J. Chem. Phys.* **1990**, *92*, 2464.
(97) Frenking, G.; Koch, W.; Cremer, D.; Gauss, J.; Liebman, J. F. *J. Phys. Chem.* **1989**, *93*, 3397.
(98) Frenking, G.; Koch, W.; Cremer, D.; Gauss, J.; Liebman, J. F. *J. Phys. Chem.* **1989**, *93*, 3410.
(99) Huber, K. P.; Herzberg, G. *Constants of Diatomic Molecules*; Van Nostrand Reinhold: New York, 1979.
(100) Tatewaki, H.; Tanaka, K.; Ohno, Y.; Nakamura, T. *Mol. Phys.* **1984** *53*, 233
(101) Leung, A. W. K.; Bellert, D.; Julian, R. R.; Breckenridge, W. H. *J. Chem. Phys.* **1999**, *110*, 6298.
(102) Leung, A. W. K.; Julian, R. R.; Breckenridge, W. H. *J. Chem. Phys.* **1999**, *110*, 8443.
(103) Hayes, T.; Bellert, D.; Buthelezi, T.; Brucat, P. J. *Chem. Phys. Lett.* **1998**, *287*, 22.
(104) Bellert, D. Ph.D. Thesis, University of Florida, 1998.
(105) Bellert, D.; Buthelezi, T.; Dezfulian, K.; Hayes, T.; Brucat, P. J.*Chem. Phys. Lett.* **1996**, *260*, 458.
(106) Reddic, J. E.; Duncan, M. A. *J. Chem. Phys.* **1999**, *110*, 9948.
(107) Lei, J.; Dagdigian, P. J. *Chem. Phys. Lett.* **1999**, *304*, 317.
(108) Carrington, A.; Leach, C. A.; Marr, A. J.; Shaw, A. M.; Hutson, J. M.; Viant, M. R. *J. Chem. Phys.* **1995**, *102*, 2379.
(109) Leung, A. W. K.; Breckenridge, W. H. *J. Chem. Phys.* **1999**, *111*, 9197.
(110) *Handbook of Chemistry and Physics*, 74th ed.; Lide, D. R., Ed.; CRC Press: Boca Raton, 1993.
(111) Mason, E. A.; McDaniel, E. W. *Transport Properties in Gases*; Wiley: New York, 1988.
(112) Patil, S. H.; Tang, K. T. *J. Chem. Phys.* **1997**, *106*, 2298.
(113) Koutselos, A. D.; Mason, E. A.; Viehland, L. A. *J. Chem. Phys.* **1990**, *93*, 7125.
(114) Cambi, R.; Cappalletti, D.; Linti, G.; Pirani, F. *J. Chem. Phys.* **1991**, *95*, 1852.
(115) Adelman, S. A.; Szabo, A. *J. Chem. Phys.* **1973**, *58*, 687.
(116) Schwerdtfeger, P.; Bowmaker, G. A. *J. Chem. Phys.* **1994**, *100*, 4487.
(117) Partridge, H.; Bauschlicher, C. W., Jr. *J. Phys. Chem.* **1994**, *98*, 2301. Note that the relative asymptotic $Fe^+(^4F)/Fe^+(^6D)$ energies in Figures 3 and 4 are inconsisent with each other as well as being inconsistent with the *J*-weighted experimental value (the other figures appear to be approximately correct); see note in ref 135.
(118) Goebel, D.; Hohm, U.; Maroulis, G. *Phys. Rev. A* **1996**, *54*, 1973.
(119) Dalgarno, A. *Adv. Phys.* **1962**, *11*, 281.
(120) Aquilanti, V.; Cappelletti, D.; Pirani, F. *Chem. Phys.* **1996**, *209*, 299.
(121) Bishop, D. M.; Cybulski, S. M. *Chem. Phys. Lett.* **1993**, *211*, 255.
(122) Shelton, D. P. *Phys. Rev. A* **1990**, *42*, 2578.
(123) Koutselos, A. D.; Mason, E. A. *J. Chem. Phys.* **1986**, *85*, 2154.
(124) Kemper, P. R.; Hsu, M.-T.; Bowers, M. T. *J. Phys. Chem.* **1991**, *95*, 10600.

(125) Khan, F. A.; Clemmer, D. E.; Schultz, R. H.; Armentrout, P. B. *J. Phys. Chem.* **1993**, *97*, 7978.
(126) Schultz, R. H.; Armentrout, P. B. *J. Phys. Chem.* **1993**, *97*, 596.
(127) Khan, F. A.; Steele, D. A.; Armentrout, P. B. *J. Phys. Chem.* **1995**, *99*, 7819.
(128) Sievers, M. R.; Armentrout, P. B. *J. Phys. Chem.* **1995**, *99*, 8135.
(129) von Helden, G.; Kemper, P. R.; Hsu, M.-T.; Bowers, M. T. *J. Chem. Phys.* **1991**, *96*, 6591.
(130) Lessen, D. E.; Asher, R. L.; Brucat, P. J. *Chem. Phys. Lett.* **1991**, *177*, 380.
(131) Asher, R. L.; Bellert, D.; Buthelazi, T.; Lessen, D.; Brucat, P. J. *Chem. Phys. Lett.* **1995**, *234*, 119.
(132) Buthelazi, T.; Bellert, D.; Hayes, T.; Brucat, P. J. *Chem. Phys. Lett.* **1996**, *262*, 303.
(133) Tjelta, B. J.; Armentrout, P. B. *J. Phys. Chem. A* **1997**, *101*, 2064.
(134) Dietorle, M.; Harvey, J. N.; Heinemann, C.; Schwarz, J.; Schröder, D.; Schwarz, H. *Chem. Phys. Lett.* **1997**, *277*, 399.
(135) Heinemann, C.; Schwarz, J.; Koch, W.; Schwarz, H. *J. Chem. Phys.* **1995**, *103*, 4551. These authors also suggest that the "true" ground states of the Fe^+Rg ions (Rg = Ar, Kr, Xe) may be the $^4\Phi$ states correlating with the first Fe^+ excited state, $Fe^+(3d^7\ ^4F)$.
(136) Velegrakis, M.; Froudakis, G. E.; Farantos, S. C. *J. Chem. Phys.* **1998**, *109*, 4687.
(137) Velegrakis, M.; Froudakis, G. E.; Farantos, S. C. *Chem. Phys. Lett.* **1999**, *302*, 595.
(138) Asher, R. L.; Bellert, D.; Buthelezi, T.; Brucat, P. J. *Chem. Phys. Lett.* **1994**, *227*, 277.
(139) Ilias, M.; Neogrady, P. *Chem. Phys. Lett.* **1999**, *309*, 441.
(140) Heinemann, C.; Schwarz, H.; Koch, W. *Mol. Phys.* **1996**, *89*, 473.
(141) Haynes, C. L.; Armentrout, P. B.; Perry, J. K.; Goddard, W. A., III *J. Phys. Chem.* **1995**, *99*, 6340.
(142) Koyanagi, G. K.; McMahon, T. B. Private communication reported in ref 140.
(143) Carrington, A.; Pyne, C. H.; Shaw, A. M.; Taylor, S. M.; Hutson, J. M.; Law, M. M. *J. Chem. Phys.* **1996**, *105*, 8602.
(144) Hariharan, P. C.; Staemmler, V. *Chem. Phys.* **1976**, *15*, 409.
(145) Rigby, M.; Smith, E. B.; Wakeham, A.; Maitland, G. C. *The Forces Between Molecules*; Clarendon Press: Oxford, 1986.
(146) Gray, C. G.; Gubbins, K. E. *Theory of Molecular Fluids*; Clarendon Press: Oxford, 1984; Vol. 1 (Fundamentals).
(147) Dabrowski, I.; Herzberg, G.; Yoshino, K. *J. Mol. Spectrosc.* **1981**, *89*, 491.
(148) Siska, P. E. *J. Chem. Phys.* **1986**, *85*, 7497.
(149) Dabrowski, I.; Herzberg, G. *J. Mol. Spectrosc.* **1978**, *73*, 183.
(150) Soldan, P.; Lee, E. P. F.; Wright, T. G. *Mol. Phys.* **1999**, *97*, 139.
(151) Koskinen, J. T.; Cooks, R. G. *J. Phys. Chem. A* **1999**, *103*, 9565.
(152) Brock, L. R.; Duncan, M. A. *J. Chem. Phys.* **1995**, *103*, 9200.
(153) Reddic, J. E.; Pullins, S. H.; Duncan, M. A. *J. Chem. Phys.* **2000**, *112*, 4974.
(154) Kello, V.; Sadlej, A. J. *Theor. Chem. Acta* **1996**, *94*, 93.
(155) Leung, A. W. K.; Julian, R. R.; Breckenridge, W. H. *J. Chem. Phys.* **1999**, *111*, 4999.
(156) Hougen, J. T. *J. Mol. Spectrosc.* **1972**, *42*, 381.
(157) The atomic quadrupole moment outputs from Gaussian 98 (*XX*, *YY*, *ZZ*), are the expectation values of X^2, Y^2, Z^2 multiplied by −1 (in atomic units). Because the symmetry axis has been picked to be the *X*-axis in Gaussian 98, the standard "Q_{zz}" (unique traceless tensor) value is therefore $YY - XX$ in terms of Gaussian outputs, since $Q = -{}^1/_2[3(XX) - R^2] = -{}^1/_2[3(XX) - XX - YY - ZZ]$, and $YY = ZZ$.
(158) $\langle r_{nd}^2 \rangle$ values calculated using an efficient numerical Hartree−Fock computer program, see: Froese-Fischer, C. *The Hartree−Fock Method for Atoms. A Numerical Approach*; Wiley-Interscience: New York, 1977.
(159) Harrison, J. F. Manuscript in preparation (MCSCF calculations).
(160) Kirschner, K. N. *J. Chem. Phys.* **2000**, *112*, 10228.
(161) Bernath, P. F. *Spectra of Atoms and Molecules;* Oxford University Press: New York, 1995; p 206.
(162) Matsika, S.; Pitzer, R. M. *J. Phys. Chem. A* **1998**, *102*, 1652 and references therein.
(163) B_e' (and thus R_e') was estimated from the ω_e', $\omega_e x_e'$ values and a single $B_{v'}$ value determined by Duncan and co-workers by using the Pekeris approximation, which relates α_e', ω_e', and $\omega_e x_e'$ for a Morse potential curve (ref 161), and $B_{v'} = B_e' - \alpha_e'(v' + {}^1/_2)$. A Morse curve should be a good representation of the potential curve down to the bottom of the potential well since the $\Delta G_{v+1/2}$ values follow a linear Birge−Sponer plot.
(164) Yourshaw, I.; Zhao, Y.; Neumark, D. M. *J. Chem. Phys.* **1996**, *105*, 351, and references therein.
(165) Chalasinski, G. Private communication.
(166) Basch, H.; Julienne, P. S.; Krauss, M.; Rosenkrantz, M. E. *J. Chem. Phys.* **1980**, *73*, 6247.
(167) Breckenridge, W. H.; Jouvet, C.; Soep, B. In *Advances in Metal and Semiconductor Clusters*; Duncan, M., Ed.; JAI Press: Greenwich, 1995; Vol. 3, and references therein.
(168) Burns, K. L.; Bellert, D.; Leung, A. W.-K.; Breckenridge, W. H. *J. Chem. Phys.* **2001**, *114*, 2996.
(169) Burns, K. L.; Bellert, D.; Leung, A. W.-K.; Breckenridge, W. H. *J. Chem. Phys.* **2001**, *114*, 7877.
(170) Bauschlicher, C. W., Jr.; Langhoff, S. R. *Int. Rev. Phys. Chem.* **1990**, *9*, 149 and references therein.
(171) Lefebvre-Brion, H.; Field, R. W. *Perturbations in the Spectra of Diatomic Molecules*; Academic Press: Orlando, 1986.
(172) Lee, C. J.; Havey, M. D. *Phys. Rev. A* **1991**, *43*, 6066.
(173) Brühl, B.; Zimmerman, D. *Chem. Phys. Lett.* **1995**, *233*, 455.
(174) Brühl, R.; Kapetanakis, J.; Zimmerman, D. *J. Chem. Phys.* **1991**, *94*, 5865.
(175) Baumann, P.; Zimmerman, D.; Brühl, R. *J. Mol. Spectrosc.* **1992**, *155*, 277.
(176) Schmieder, R. W.; Lurio, A.; Happer, W. *Phys. Rev. A* **1971**, *3*, 1209.
(177) Soldan, P.; Lee, E. F. P.; Lozeille, J.; Murrell, J. N.; Wright, T. G. *Chem. Phys. Lett.* **2001**, *343*, 429.
(178) Eford, J. T.; Roeggen, I.; Skullerud, H. R. *J. Phys. B.* **1999**, *32*, 1873.
(179) Soldan, P.; Lee, E. P. F.; Lozeille, J.; Wright, T. G. Unpublished results. (High-level ab initio calculations with very large basis sets; ω_e values for isotopes ^{7}Li, ^{23}Na, ^{39}K, ^{4}He, ^{20}Ne, ^{40}Ar, ^{84}Kr, ^{132}Xe.)
(180) Bauschlicher, C. W., Jr.; Langhoff, S. R.; Partridge, H. In *Modern Electronic Structure Theory*; Yarkony, D. R., Ed.; World Scientific: Singapore, 1995.
(181) Massaouti, M.; Sfounis, A.; Velegrakis, M. *Chem. Phys. Lett.* **2001**, *348*, 47.
(182) Angel, J. R. P.; Sandars, P. G. H.; Woodgate, G. K. *J. Chem. Phys.* **1967**, *47*, 1552.
(183) Basch, H.; Julienne, P. S.; Krauss, M.; Rosenkrantz, M. E. *J. Chem. Phys.* **1980**, *73*, 6247.
(184) Weltner, W., Jr. *Magnetic Atoms and Molecules*; Dover: New York, 1983, p 59.

CR980090E